arXiv:2609.03571v1 [cond-mat.soft] 3 Sep 2026

Heterogeneous collapse in thermoresponsive copolymer microgels varying molar composition

Jacopo Vialetto,[*,†,‡] Francesco Brasili,[¶,§] Letizia Tavagnacco,[¶,§] Gavino Bassu,[†,‡] Elena Buratti,[‖] Stephen King,[⊥] Emanuela Zaccarelli,[*,¶,§] and Marco Laurati[*,†,‡]

†*Department of Chemistry, University of Florence, via della Lastruccia 3, Sesto Fiorentino, I-50019 Firenze, Italy*

‡*Consorzio interuniversitario per lo sviluppo dei Sistemi a Grande Interfase (CSGI), via della Lastruccia 3, 50019 Sesto Fiorentino (FI), Italy*

¶*Institute for Complex Systems, National Research Council, Piazzale Aldo Moro 5, 00185, Roma, Italy*

§*Department of Physics, Sapienza University of Rome, Piazzale Aldo Moro 5, 00185 Roma, Italy*

‖*Department of Environmental and Prevention Sciences, University of Ferrara, Via L. Borsari, 46, 44121 Ferrara, Italy*

⊥*ISIS Neutron and Muon Source, Rutherford Appleton Laboratory, Oxfordshire, OX11 0QX, UK*

E-mail: jacopo.vialetto@unifi.it; emanuela.zaccarelli@cnr.it; marco.laurati@unifi.it

Abstract

Understanding the internal architecture of copolymer microgels is crucial for establishing how nanoscale polymer organization controls their stimuli-responsive behavior. Here we focus on thermoresponsive P(N-isopropylacrylamide-*co*-N-isopropylmethacrylamide), P(NIPAM-*co*-NIPMAM), microgels with varying mole fraction of the

components, synthesized via radical precipitation polymerization, and we demonstrate that changes in their volume phase transition and equilibrium swelling are governed by composition-dependent internal heterogeneity. Comparison between small-angle neutron scattering (SANS) with isotopic labeling and monomer-resolved simulations show a block-like monomer distribution of the two components. SANS analysis reveals a universal maximum in the polymer mesh correlation length near the transition, evidencing coexistence of collapsed NIPAM-rich and swollen domains. The correlation length increases with increasing NIPMAM content, with a maximum for 75 mol % NIPMAM, implying sparse collapsed regions within the network and thus a large degree of heterogeneity induced by the presence of an increasingly large fraction of intercalated, non-collapsing PNIPMAM. The maximum heterogeneity correlates with the equilibrium swelling ratio, indicating that collapsed microgels retain a structural memory of the transition and present a less-compliant structure in response to temperature variations. Overall, these insights highlight a complex effect of the block-like monomer distribution on the responsive properties of copolymer microgels with different compositions, thus providing a design rule for tailoring responsive colloids for functional soft materials.

Introduction

Stimuli-responsive colloids are an important class of materials with significant interest for fundamental studies in condensed matter physics, and for multiple potential applications ranging from drug delivery to additive manufacturing or surface coatings.[1–4] In particular, colloids made of crosslinked polymeric networks (i.e. microgels) offer a platform potentially responsive to multiple stimuli (pH, temperature, light, specific molecules, etc.) that can be tailored to the users needs by choosing the network components. The most studied systems include the thermoresponsive polymer poly(N-isopropylacrylamide) (PNIPAM). PNIPAM microgels undergo a volume phase transition (VPT) at a critical temperature

($T_{VPT} \simeq 32°C$), from a swollen to a collapsed particle due to a decrease of solvent affinity of the polymer.[5] Superior control over microgel's responsiveness to various stimuli can be achieved by incorporating a second polymer during the particle synthesis.[6] Copolymerization of PNIPAM microgels provides pH or light responsiveness,[7–10] or it allows tuning T_{VPT} to meet the required functions. In particular, comonomers such as N-isopropylmethacrylamide (NIPMAM),[11,12] N-n-propylacrylamide (NnPAM)[13] or oligo(ethylene glycol) methyl ether methacrylate (OEGMA)[14–18] allow increasing pure PNIPAM T_{VPT} to match the body temperature, of interest for applications such as drug delivery and tunable cell adhesion, where specific functions can be tuned in physiological conditions.[19]

An important aspect controlling microgel responsivity and interactions is the architecture of the polymeric network. Different responses can be achieved when two (or more) polymers are spatially separated, one in the core and one in the shell of the particle, as in core-shell microgels, or if the microgels are synthesized with statistical copolymerization. In core-shell microgels two distinct T_{VPT} are present, corresponding to the collapsing temperature of each of the homopolymer region of the particle.[20–22] If instead the two monomers are added together during particle synthesis (i.e. one-pot synthesis), one single T_{VPT} is typically obtained.[13,23] In such cases, the relative distribution of the components within the polymeric network will depend on the reaction constants[24,25] and on the interactions between the polymer chains. Although this will ultimately dictate the overall network response and is fundamental in order to predict material properties, to date little information is known on the detailed internal copolymer distribution as most techniques do not provide access to this information. Additionally, even more basic properties, such as the dependence of T_{VPT} on composition, are not straightforward. For example, in PNIPAM-PNIPMAM microgels T_{VPT} changes linearly with PNIPMAM content.[12] Instead, for poly(N-vinylcaprolactam) PVCL-PNIPMAM particles, Balaceanu and coworkers showed that T_{VPT} increases non-linearly from 34°C to 45°C upon increasing the PNIPMAM fraction, with the behavior of copolymer microgels made with ratios higher or lower than 1 dominated by VCL or NIPMAM, re-

spectively.[23] This indicates that the specific interactions between the monomers might yield significantly different results and that a precise characterization of these systems is required in order to expand their applicability in various fields.

Here, we focus on the well-known P(NIPAM-*co*-NIPMAM) system. PNIPMAM, displaying a $T_{VPT} \simeq 44°C$,[26] allows modulation of the transition temperature in copolymer networks in the physiological range.[12,27] A previous work analyzed microgels at equimolar composition, observing that the T_{VPT} of the copolymer network is $38°C$ and thus in between that of the corresponding homopolymers.[11] Recently, by combining small-angle neutron scattering (SANS) and nuclear magnetic resonance (NMR) experiments with numerical simulations, we probed the swelling behavior of the microgels at equimolar composition across T_{VPT} unveiling the formation of local domain structures (named block topology) within the network. These domains are composed of repeating units of the same type (either NIPAM or NIPMAM), which preferentially cluster together rather than being randomly and homogeneously distributed.[28] These results indicate that the internal conformation of copolymer microgels is not necessarily a simple statistical distribution, even in a one-pot synthesis, and that such compositional heterogeneity can be revealed only by probing the inner structure of the particles. Taking a step further, here we investigate P(NIPAM-*co*-NIPMAM) microgels at varying composition by combining dynamic light scattering (DLS), differential scanning calorimetry (DSC), SANS and numerical simulations to characterize their internal structure and thermal responsivity, and we evidence that such internal heterogeneity is composition dependent, reaching a maximum for 75 mol % PNIPMAM. The heterogeneity at the transition temperature are reflected in variations in the equilibrium swelling ratio, suggesting that the collapsed microgels preserve a structural signature of the transition, which modulates their temperature response and deswelling.

Materials and methods

Reagents

N-isopropylacrylamide (NIPAM, MW = 113.16 Da, Sigma, 97% purity), N-isopropylmethacrylamide (NIPMAM, MW = 127.18 Da, Sigma, 97% purity), N,N'-methylenebisacrylamide (BIS, MW = 154.17 Da, Sigma, 99% purity), Sodium dodecyl sulfate (SDS, MW = 288.38 Da, Sigma, 99% purity) potassium persulfate (KPS, MW = 270.32 Da, Sigma, 99% purity) and deuterium oxide (Sigma, 99.9 atom % D). NIPAM and NIPMAM were purified by recrystallization in hexane. Water used for all experiments is bi-distilled Milli-Q.

Microgel synthesis

The microgels used in this work were synthesized by radical precipitation polymerization. We used 5% BIS as crosslinker and 1% KPS as initiatior. The reaction was carried out in a solution with 4 mM SDS surfactant. We used different molar percentage of the NIPAM and NIPMAM monomers, as reported in Table 1. Briefly, the monomers, crosslinker and surfactant were dissolved in 26.5 mL of deionized water to yield final concentrations of 160 mM, 8 mM, and 4 mM, respectively. The solution was loaded in a 50 mL two-necked reactor equipped with a condenser and a magnetic stirrer, and then bubbled under a nitrogen stream for 1 hour at room temperature. Separately, the initiator was dissolved in degassed water at the concentration of 36.9 mM. The temperature in the reactor was raised to 70°C using an oil bath and then the polymerization reaction was initiated by adding 1.2 mL of the initiator solution at the rate of 1 mL/min. The final concentration of the initiator in the reaction solution was 1.6 mM. The reaction was carried out for 5 hours. The resulting microgels were purified by dialysis against ultrapure water using a cellulose membrane (6–8 kDa MWCO, Sigma) for two weeks, with the water replaced twice daily. The microgel solutions were then freeze-dried and stored in the dark at 4°C.

For the synthesis of microgels with deuterated NIPAM, P(D-NIPAM-co-H-NIPMAM)

with 25% NIPAM and 75% NIPMAM monomers, we used 8 mol% H-NIPAM and 17 mol% NIPAM-d_{10}, while keeping the same molar concentrations of the other reagents and synthesis procedure. The PNIPAM composition is chosen in order to match the scattering length density with that of the solvent. NIPAM-d_{10} monomers were synthesized at the Jülich Centre for Neutron Scattering according to the procedure reported in ref. 28.

Table 1: Microgels used in this work

Microgel	NIPAM mol %	NIPMAM mol %	R_h (20°C) [nm]	$\frac{R_h(25°C)}{R_h(T_{max}\ °C)}$	VPTT [°C]
M_{100-0}	100	0	58.5 ± 0.4	1.97 ± 0.03	33.1 ± 0.1
M_{75-25}	75	25	72.5 ± 0.2	1.93 ± 0.02	35.0 ± 0.1
$M_{62.5-37.5}$	62.5	37.5	81.0 ± 0.7	1.91 ± 0.02	36.1 ± 0.1
M_{50-50}	50	50	79.4 ± 0.3	1.87 ± 0.01	37.9 ± 0.1
$M_{37.5-62.5}$	37.5	62.5	68.4 ± 0.8	1.81 ± 0.02	39.2 ± 0.1
M_{25-75}	25	75	96.5 ± 0.5	1.79 ± 0.01	40.9 ± 0.1
M_{0-100}	0	100	95.5 ± 0.5	1.91 ± 0.02	44.4 ± 0.1

Experimental methods

Dynamic light scattering. Dynamic light scattering (DLS) experiments were performed using a Zetasizer PRO Red Label (Malvern, UK). The microgels were redispersed in Milli-Q water at a concentration of 0.01 wt% in order to analyze them in the dilute regime. The temperature was varied from 25 to 50°C or 65°C with 1°C steps and 5 minutes equilibration time. For each temperature we recorded three consecutive intensity autocorrelation functions, each averaged over 20 runs. We then extrapolated decay times by cumulant analysis of the correlograms, and derived the distribution of diffusion coefficients D of the microgels. Intensity-weighted distributions of hydrodynamic radius R_h were obtained using the Stokes-Einstein relationship $R_H = k_BT/6\pi\eta D$, where k_BT is the thermal energy and η the water viscosity. The temperature-responsive change in hydrodynamic radius $R_h(T)$ was fitted to the phenomenological function[29,30]

$$R_h(T) = R_0 - \Delta R \tanh\left[s\left(T - T_{VPT}\right)\right] + A\left(T - T_{VPT}\right) + B\left(T - T_{VPT}\right)^2 \quad , \qquad (1)$$

where $R_0 = \frac{1}{2}(R_{\max}+R_{\min})$ and $\Delta R = \frac{1}{2}(R_{\max}-R_{\min})$, with $R_{\max}$ and $R_{\min}$ the plateau values of $R_h(T)$ at low (fully swollen microgels) and high (fully collapsed microgels) temperatures, respectively, T_{VPT} is the critical temperature of the VPT, s is the sharpness parameter, whose inverse quantifies the temperature range over which the VPT occurs. The linear and quadratic terms, whose fitting coefficients are A and B, respectively, are phenomenological corrections that allow to accurately reproduce the non-flat baselines of the experimental trends outside the temperature range of the VPT, occurring in particular at low temperatures. In this way, the function is able to accurately capture the behavior of $R_h(T)$ in the whole investigated temperature range, avoiding spurious effects on the physical parameters such as T_{VPT} and s.

We also defined the experimental swelling ratio SR_{exp} as the ratio between the hydrodynamic radii $R_h(25°\text{C})$ and $R_h(T_{max})$, in swollen and collapsed conditions, respectively:

$$SR_{exp} = \frac{R_h(25°\text{C})}{R_h(T_{max})} \tag{2}$$

In order to account for fully collapsed particles, we selected T_{max} well-above T_{VPT} for all the analyzed samples. Specifically, $T_{max} = 50°\text{C}$ up to 37.5 mol % NIPMAM and $T_{max} = 65°\text{C}$ for samples with larger NIPMAM content.

Differential scanning calorimetry (DSC). Thermal analyses on microgels were performed with a Perkin Elmer Pyris Diamond DSC equipped with Intracooler III as cooling system and a DSC 8000 Perkin Elmer differential scanning calorimeter equipped with Intracooler II as cooling system. About 10 mg of microgel dispersions at $C_w = 10$ wt% was analysed under nitrogen atmosphere (20 mL/min) in hermetic sealed steel pans. The measurements were carried out by cooling the system from 20 to 0 °C, holding the temperature for 1 min, then heating it to 80 °C, holding the temperature for 1 min and finally by cooling it again to 20 °C. Each cooling and heating step was carried out with a scanning rate of 5 °C/min. Analysis of the thermograms was performed with *Pyris 7* software.

Small-angle neutron scattering (SANS). Mixtures of microgels (0.1 w/w %) were prepared by diluting stock solutions of freeze-dried microgels in D_2O. The obtained samples were then mixed at room temperature in an orbital shaker overnight. SANS measurements were performed at SANS2D (ISIS, Didcot, UK) and SANS-I (PSI, Villigen, Switzerland) beamlines. At SANS2D we used a white beam of wavelength $1.75 < \lambda < 12.5$ Å , an incident collimation of 12 m and two detectors placed 5 and 12 m from the sample. These settings gave a simultaneous wave vector range of 0.0015 Å$^{-1} < Q < 0.50$ Å^{-1}. While at SANS-I we used a constant $\lambda = 8$ Å for three sample-to-detector distances of 1.6 m, 4.5 m and 18 m, and collimations of 3, 4.5 and 18 m, respectively. The combination of the three configurations gave a wave vector range of 0.0018 Å$^{-1} < Q < 0.25$ Å^{-1}.

All samples were measured at different temperatures between 20°C and 50°C in quartz cells with a path length of 2 mm (Hellma GmbH & Co., Mullheim, Germany). After reaching the desired temperature, the samples were equilibrated for at least 5 min. All scattering data were normalized for the sample transmission and background corrected using a quartz cell filled with D_2O. All data were analyzed within the SASView package (version 5.0.6, 10.5281/zenodo.7581379) using user-written functions. The SANS scattered intensities of the microgel suspensions can be expressed as:

$$I(q) = \phi V (\Delta\rho)^2 P(q) S(q) + \text{bkg} \tag{3}$$

where ϕ is the microgel volume fraction, V the microgel volume, $\Delta\rho = \rho_1 - \rho_2$ the scattering length density difference between the microgels (ρ_1) and D_2O (ρ_2), $P(Q)$ the particle form factor, S(Q) the interparticle structure factor and bkg the background.

$P(Q)$ was described using the well-known fuzzy sphere model from Stieger et al.:[31]

$$P(q) = A_1 \left[\frac{3[sin(qR) - qRcos(qR)]}{(qR)^3} \cdot \exp\left(-\frac{(\sigma q)^2}{2}\right) \right]^2 + A_2 \frac{1}{1 + (q\zeta)^2} \tag{4}$$

where the first term models the fuzzy sphere contribution, with R the particle radius and σ

the fuzziness parameter, while the second term describes the polymer network scattering in the region at high Q, with ζ the correlation length of the polymer mesh. The contributions of the two terms are weighted by the amplitudes A_1 and A_2.

For samples with low effective microgel concentration (e.g. M_{25-75} in Figure 2), the structure factor contribution is negligible and therefore $S(Q) = 1$. Instead, for samples with a noticeable structure factor (for instance M_{75-25} in Figure S11 of the SI), we modeled the $S(Q)$ contribution using a hard-sphere structure factor calculated using the Percus-Yevick closure relationship and containing two parameters, an effective hard-sphere radius R_{HS} and an effective hard-sphere packing fraction φ_{HS}. We should note that our focus is on extracting changes in the particle morphology associated with the VPTT and as a function of the microgel composition. For this reason we decided to use a simple hard-sphere model to describe the shape of the experimental S(Q) rather than a more accurate description using the Hertzian interaction potential, as done in previous work.[32] For the fits, the model function was convoluted with the following experimental smearing function:

$$I(q) = \int P(q - q') \left(\frac{1}{2\pi\sigma_{q'}^2} \right)^{1/2} \exp\left[-\frac{q'^2}{2\sigma_{q'}^2} \right] \mathrm{d}q' \tag{5}$$

where σ_q is the standard deviation of the q resolution, which contains the detector resolution and the beam wavelength spread contributions.[33] In addition, sample polydispersity was included considering a Schulz distribution of the radius.

Numerical simulations

We perform monomer-resolved simulations of copolymer microgels obtained following an *in silico* synthesis protocol[34] which provides a realistic description of the disordered network and the fuzzy sphere structure.[35] We employ copolymer microgels with a *block* topology, where each polymer chain included between two cross-linkers is entirely assigned to a PNIPAM or PNIPMAM homopolymeric segment. Indeed, this topology was shown to be the most

accurate to reproduce the experimental data.[28] Microgels are composed by $N \sim 42000$ beads. NIPAM and NIPMAM repeating units are described by bivalent patchy particles, while cross-linkers have four attractive patches. The experimental conditions are reproduced by setting the crosslinker concentration to $c = 5.0\%$ and by using copolymer ratios from 0 to 100.

Beads composing the polymer network interact with the Kremer-Grest potential,[36] thus, experiencing a steric repulsion modelled by the Weeks-Chandler-Anderson (WCA) potential:

$$V_{\mathrm{WCA}}(r) = \begin{cases} 4\varepsilon \left[\left(\frac{\sigma}{r}\right)^{12} - \left(\frac{\sigma}{r}\right)^{6} \right] + \varepsilon & \text{if} \quad r \leq 2^{\frac{1}{6}}\sigma \\ 0 & \text{if} \quad r > 2^{\frac{1}{6}}\sigma \end{cases} \tag{6}$$

where ϵ and σ are the energy and length units, respectively. In addition, bonded beads interact via the finitely extensible nonlinear elastic potential (FENE):

$$V_{\mathrm{FENE}}(r) = -\varepsilon k_F R_0^2 \log \left[1 - \left(\frac{r}{R_0 \sigma} \right)^2 \right] \qquad r < R_0\sigma \tag{7}$$

where $R_0\sigma$ is the maximum bond distance and k_F is a stiffness parameter that determines the bond rigidity. The covalent nature of the network is accounted for by excluding that bonds can break during the simulation.

The solvent effect is implicitly included by using an effective potential which reproduces the change in the polymer-solvent affinity by raising temperature:

$$V_{\alpha}(r) = \begin{cases} -\varepsilon\alpha & \text{if} \quad r \leq 2^{\frac{1}{6}}\sigma \\ \frac{1}{2}\alpha\varepsilon \left\{ \cos\left[\gamma \left(\frac{r}{\sigma}\right)^2 + \beta \right] - 1 \right\} & \text{if} \quad 2^{\frac{1}{6}}\sigma < r \leq R_0\sigma \\ 0 & \text{if} \quad r > R_0\sigma \end{cases} \tag{8}$$

where α is the solvophobicity parameter corresponding to the effective temperature. The swelling curve of the microgels is obtaining by changing the value of α from good ($\alpha = 0$)

to bad ($\alpha = 1.5$) solvent conditions. Here $\gamma = \pi \left(\frac{9}{4} - 2^{\frac{1}{3}}\right)^{-1}$ and $\beta = 2\pi - \frac{9}{4}\gamma$ are constants defining the functional shape of the potential.[37]

The bead size is set to $\sigma = 1$ for NIPAM and $\sigma = 1.04$ for NIPMAM to mimic their steric volume difference. Furthermore, the different volume phase transition temperature for PNIPAM and PNIPMAM microgels is modelled by using a different value of α for each monomer, based on the relation between α and temperature determined for PNIPAM microgels in Ref. 34. For mixed interactions occurring between NIPAM and NIPMAM beads the average value of α is used. The value of α reported in the manuscript always refers to the PNIPAM α-value for convenience.

Simulations are carried out with the LAMMPS package[38] in a cubic box with side L $= 200\ \sigma$ at a fixed temperature $\frac{k_B T}{\epsilon} = 1.0$. Equations of motion are integrated through a Nosé–Hoover thermostat in the constant NVT ensemble with an integration time-step $\Delta t = 0.002\tau$, where $\tau = \sqrt{\frac{m\sigma^2}{\varepsilon}}$ is the reduced time unit. The equilibration of each system is carried out for $1{\cdot}10^6\tau$, followed by a production run of $1{\cdot}10^7\tau$.

To directly compare numerical results to the experimental measurements, we computed the microgel form factor $P(q)$ and hydrodynamic radius R_h. $P(q)$ is given by

$$P(q) = \frac{1}{N} \sum_{ij} \langle exp(-i\vec{q} \cdot \vec{r}_{ij}) \rangle \tag{9}$$

where q is the wavevector, r_{ij} is the distance between the monomers i and j and the calculation is averaged over independent configurations. The hydrodynamic radius R_h is calculated as:[8,39]

$$R_{sim} = 2 \left[\int_0^\infty \frac{1}{\sqrt{(a^2+\theta)(b^2+\theta)(c^2+\theta)}} d\theta \right]^{-1} \tag{10}$$

where the microgel is approximated as an effective ellipsoid with semiaxes a, b and c. To compare the swelling curves of R_{sim} to the experimental ones, we normalized each value of R_{sim} to that of the same microgel in the fully swollen state ($\alpha = 0$ or $T = 25$°C). The values of α are mapped to the experimental temperatures based on the relationship reported

in ref. 28, which was optimized to reproduce the temperature-dependent evolution of the experimental form factors of the microgel M_{50-50}. However, focusing on the 50:50 copolymer composition, that calibration assumes equal contributions of NIPAM and NIPMAM to the effective temperature α. Here the different compositions of the co-polymer microgels need to be taken into account. We therefore corrected the mapping relation by introducing the relation $\alpha_f = \alpha_{0.5} - (f - 0.5)\Delta\alpha$, where $\Delta\alpha = \alpha_{\mathrm{NIPAM}} - \alpha_{\mathrm{NIPMAM}}$ is the difference between the values of the solvophobicity parameter of the two monomers and f is the molar fraction of NIPMAM.

Results and discussion

The microgels investigated in this work are synthesized by radical precipitation polymerization, mixing the two monomers NIPAM and NIPMAM in the desired amounts and in the presence of SDS surfactant. The latter is required to obtain particles with radii compatible with SANS experiments (see Materials and methods for additional details on the synthesis protocol). All microgels contain a constant amount of crosslinker: 5 mol % N,N'-methylenebis(acrylamide) (BIS). A DLS characterization of the microgels dispersed in H_2O is reported in Figure 1A and in Table 1. The evolution of the hydrodynamic radius (R_h) as a function of temperature is fitted with eq. 1 (black lines) in order to extract T_{VPT} for each NIPAM-NIPMAM composition (Figure 1B, black circles) and the parameter $1/s$, which represents the width of the transition (Figure 1C). The full set of fitting parameters is reported in Table S1. Interestingly, T_{VPT} of the copolymer microgels does not precisely match the expected value for a linear dependence with composition,[12,40] but is instead consistently approximately 1°C lower. This result is further corroborated by differential scanning calorimetry (DSC) experiments (Figure S1), with T_{VPT} determined from the onset of temperature increase in the thermograms. Despite a consistent discrepancy of approximately 3 °C between T_{VPT} obtained from DLS and DSC analysis, also with the latter we observe slightly

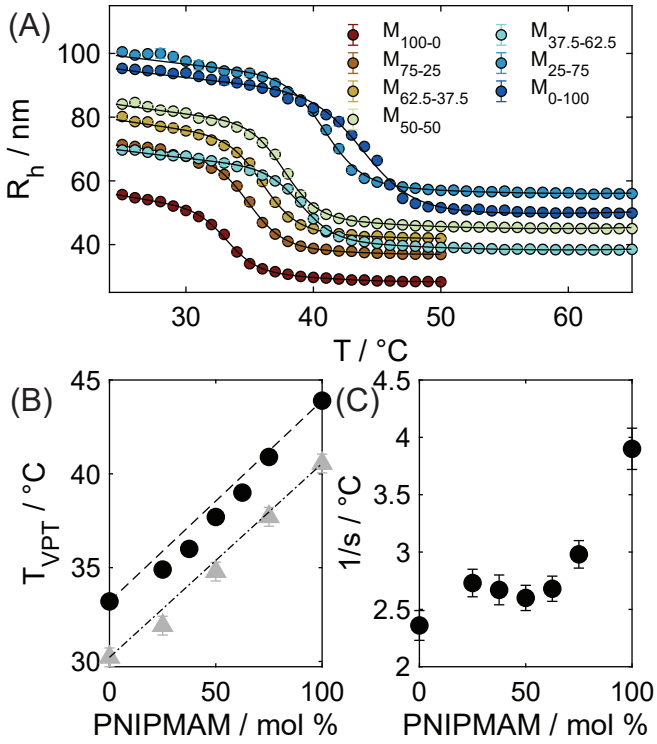


Figure 1: PNIPAM-PNIPMAM microgels: experiments. (A) Microgel hydrodynamic radii as a function of temperature. Error bars indicate the standard deviation of 3 measurements. Black lines are fits with eq. 1. (B) T_{VPT} as a function of PNIPMAM composition as obtained from DLS (black circles) and DSC (gray triangles) analysis. In some cases the error bounds are smaller than the symbol size. The dashed and dashed-dotted lines indicates the expected T_{VPT} in case of a linear dependence with the copolymer content for DSL and DSC experiments, respectively. (D) $1/s$ parameter indicating the VPT width.

lower transition temperatures for the copolymer microgels (Figure 1B, gray triangles).

Figure 1C additionally shows that the transition width increases with increasing PNIPMAM content, albeit not in a linear fashion. Regarding the homopolymer PNIPAM and PNIPMAM microgels, a broader transition for the latter captures what is observed in previous works.[26,41] Overall, these results suggest that thermal responsivity depends not only on composition but also on the internal polymer distribution. However, a standard DLS and DSC characterization does not allow for a deeper understanding of this phenomenon.

In parallel, we also exploited monomer-resolved simulations to obtain *in-silico* copolymer microgels with varying amounts of the two monomers. Representative simulation snapshots of the microgels in their swollen state are reported in Figure 2A, where M_{75-25} indicates

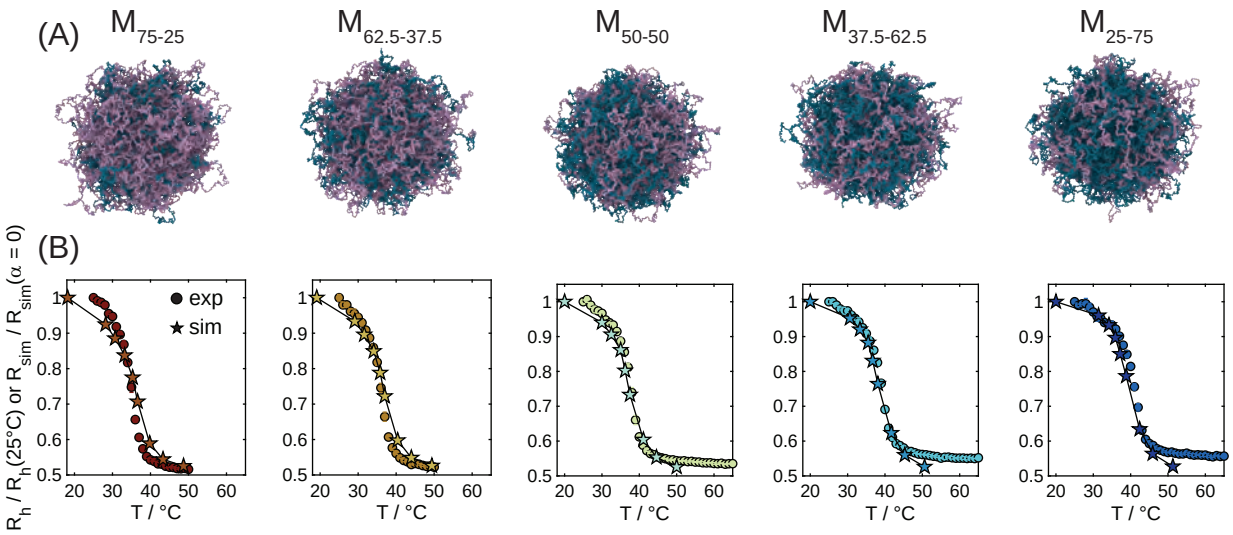


Figure 2: Numerical simulations of PNIPAM-PNIPMAM microgels. (A) Snapshots of PNIPAM-PNIPMAM microgels with different compositions (indicated). PNIPAM beads are in pink, PNIPMAM beads in green. (B) Comparison between experimental (circles) and numerical (stars) swelling curves, plotted by normalizing, for each microgel, values of R to the one in the swollen state: R_h(T = 25°C) for experiments for simulations or $R_{sim}(\alpha = 0)$. The procedure to map the solvophobic parameter α to experimental temperature T is described in the Methods.

a P(H-NIPAM-*co*-H-NIPMAM) microgel with 75 mol % NIPAM and 25 mol % NIPMAM, and so on. The simulations are performed as described in Methods, using the so-called "*block*" topology, which yielded favourable results in comparison to experiments for equimolar microgels.[28] To complement DLS and DSC, we also monitor the swelling behavior in simulations (see Materials and methods for further details). The swelling curves derived from simulations are superimposed to experimental ones in Figure 2A. To achieve a proper comparison, for each sample we normalized the hydrodynamic radius to that of the swollen microgels. Moreover, we mapped the solvophobic parameter α to experimental temperature by extending the relation previously derived in ref. 28 for microgel M_{50-50} to account for the different compositions of the samples, as detailed in the Materials and methods. Noteworthy, we found that the swelling curves obtained in this way accurately reproduce the evolution of the particle size as a function of temperature and the influence of copolymer content on the swelling behavior.

For an in-depth characterization of the internal polymer network conformation as a func-

tion of NIPMAM comonomer ratio, we performed SANS measurements of dilute suspensions in D_2O to determine the particle form factors. In Figure 3 we report the scattering intensities $I(q)$ of the exemplary M_{25-75} for temperatures spanning its VPT. SANS data for the other PNIPMAM compositions are in the Supporting Information (Figures S2-S14). The well-known fuzzy sphere model from Stieger et al.[31] (eq. 4) nicely captures the experimental form factors for all compositions and investigated temperatures. We note that in our experiments we do not discern non-thermoresponsive domains in the homopolymer cases, as recently visualized by using high-speed atomic force microscopy on bigger particles.[42,43] As shown in Figure 3A, we observe the expected decrease in size at high temperature, indicated by a right-shift of the Guinier (low-q) region of the scattering curves. This is coupled with an increase in the slope of $I(q)$ at higher q values, indicative of a transition from a more open polymer network with a diffuse interface to one that is collapsed and with a more compact interface.

The resulting particle radius from the form factor fits is plotted in Figure 3B and shows particle deswelling up to T_{VPT}, after which the microgel is collapsed and the contribution of the particle fuzziness 2σ to the total radius is significantly decreased.

While this result is in line with the form factor of commonly investigated PNIPAM microgels,[31] insight into the internal structure can be obtained by looking at the variation in the correlation length of the polymer mesh (ζ) as a function of temperature (Figure 3C). Interestingly, ζ first increases, reaching a maximum at $T = 40°C$, and then sharply decreases above T_{VPT}, which is 40.9 $\pm$ 0.1 °C for this microgel, when the network is significantly collapsed. We interpret ζ as an estimate of the average distance between heterogeneous, non collapsed regions within the network. ζ increases near T_{VPT} due to the onset of network collapse, which increases the overall heterogeneity of the microgel architecture, comprised of collapsed and still swollen domains. This trend of ζ increasing below T_{VPT} and then sharply decreasing afterwards is consistently reproduced for all investigated microgels (Figures S2-S14).

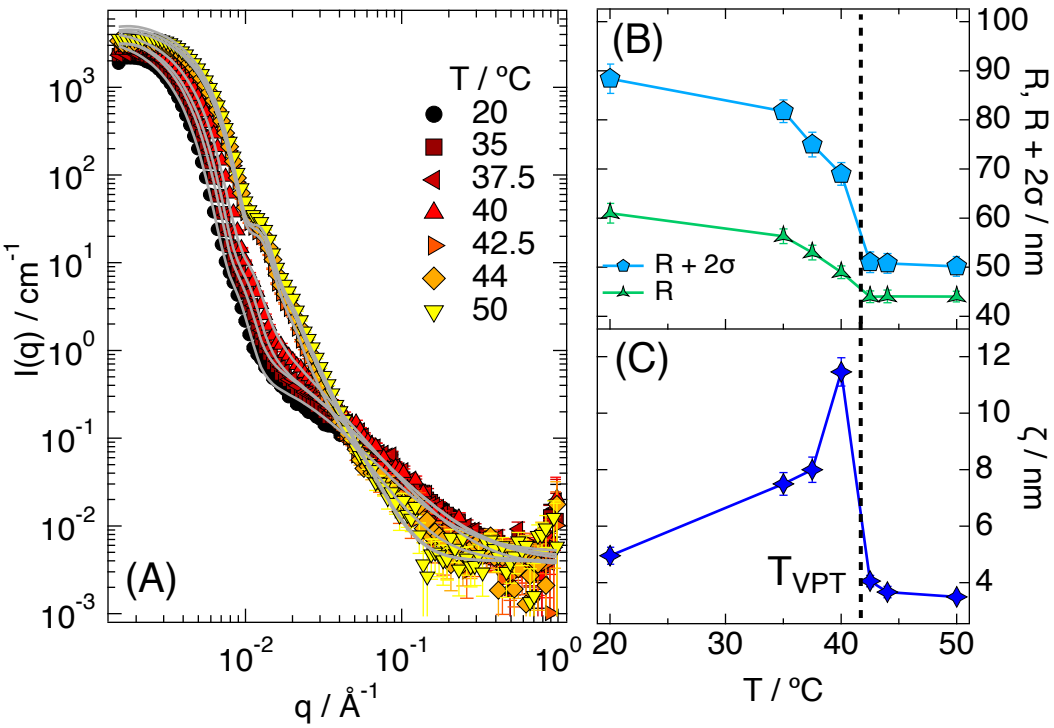


Figure 3: SANS of M_{25-75}. A) SANS scattering intensities $I(q)$ as a function of temperature. Lines represent fits with the fuzzy sphere model in eq. 4. B) Particle radii R and $R + 2\sigma$ from SANS fits as a function of temperature. C) Correlation length of the polymer mesh (ζ). In B) and C) the dashed line indicates T_{VPT} from DLS analysis.

In order to challenge the peculiar block structure made of separate PNIPAM and PNIPMAM domains that we put forward for describing the internal architecture of 50-50 P(NIPAM-*co*-NIPMAM) microgels,[28] in Figures S15 and S16 we compare experimental form factors for M_{25-75} and for a 25-75 P(D-NIPAM-*co*-H-NIPMAM) microgel, with numerical ones obtained with the *random* or *block* models (see Materials and methods for details on the comparison procedure). As previously discussed,[28] isotopic labeling of one of the two polymers for contrast matching in D_2O is mandatory in order to distinguish between *random* or *block* topologies and gain insights on the internal structure. Indeed, Figure S15 shows that both the *random* and *block* architectures capture the evolution of the form factors across T_{VPT} for the fully hydrogenated M_{25-75} sample, not being able to provide details on the internal architecture. Instead, Figure S16 highlights an excellent agreement of the numerical data in describing the microgel architecture when the *block* model is used, while the *random* model

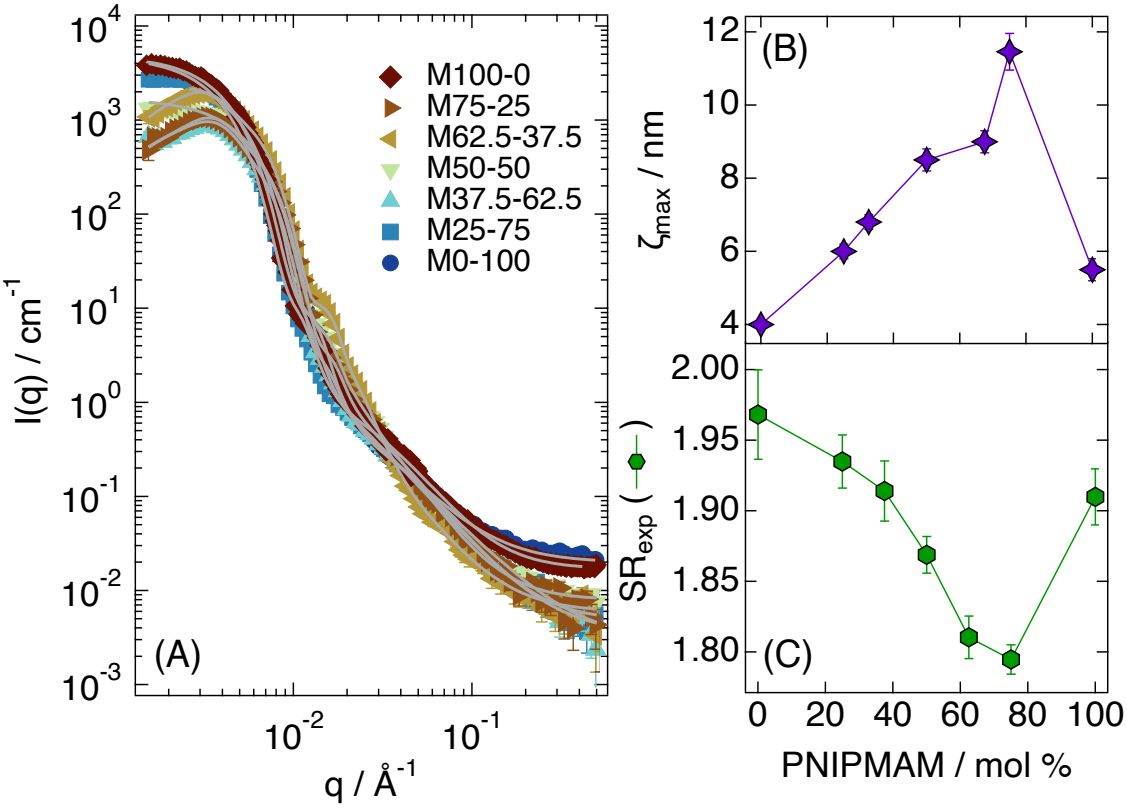


Figure 4: A) SANS scattering intensities $I(q)$ for different compositions at the temperature at which the correlation length of the polymer mesh is maximum. Lines are fits with the fuzzy sphere model. B) Maximum correlation length ζ_{max} and (C) swelling ratio from experiments (SR_{exp}) as a function of PNIPMAM mole fraction.

provides a less accurate representation of experimental data, and therefore validating the *block* topology also for P(NIPAM-*co*-NIPMAM) microgels of different composition. Additionally, the resulting ζ values are much more moderate for the D-H microgel with respect to the H-H one (Figure S17), hinting at a more homogeneous network. Since in D-H microgels in D_2O the D-PNIPAM domains are contrast-matched with the solvent and do not contribute to the scattering profile, this indicates that the PNIPMAM network is more homogeneous than the PNIPAM one, and corroborates the attribution of network heterogeneities observed in H-H microgels to the formation of PNIPAM domains at the deswelling transition.

We then investigated in detail how the NIPMAM mole fraction affects the internal polymer distribution and reorganization as a function of temperature. In Figure 4A we compare

SANS scattering intensities measured at the temperature corresponding to the maximum in the correlation length of the polymer mesh (ζ_{max}), for all investigated compositions. We note that such temperature increases with increasing NIPMAM content. As already indicated, we interpret ζ_{max} as an estimate of the average distance between non collapsed regions within the network, thereby giving information on the internal heterogeneity. The resulting ζ_{max} (Figure 4B) is the lowest for pure PNIPAM or PNIPMAM microgels, indicating that the homopolymer networks have an overall more homogeneous polymeric distribution at the VPT, as expected for particles composed of a single monomer. The discrepancy that is observed between pure PNIPAM and pure PNIPMAM microgels hints to a slight increase in network heterogeneity during collapse for the latter monomer, in line with the increased transition width (Figure 1C). In copolymer networks, ζ_{max}, by providing information on the network heterogeneity, is therefore an estimate of the average distance between NIPAM-rich domains, which collapse first due to their lower critical solution temperature with respect to PNIPMAM. Upon increasing the NIPMAM mole fraction, the average distance between collapsed NIPAM-rich blocks progressively increases. Below 50 % there is still a significant amount of NIPAM in the network, resulting in a few non-collapsed regions and an intermediate value of ζ_{max}. Instead, a further decrease in NIPAM content yields networks with only a few collapsed regions, characterized by a further increase in ζ_{max}, which reaches its maximum for M_{25-75} among the studied range of compositions.

In Figure 4C we display the microgel's experimental swelling ratio (SR_{exp}, green points) measured as the ratio between the hydrodynamic radii $R_h(25°C)/R_h(T_{max})$, where T_{max} is chosen to be well-above T_{VPT} in order to capture fully collapsed particles: 50°C up to 37.5 % NIPMAM mol fraction, 65°C for the remaining particles. Interestingly, SR_{exp} as a function of NIPMAM content mirrors the ζ_{max} trend, with a continuous decrease up to a minimum for M_{25-75}, which corresponds to the more heterogeneous structure prior to network collapse, and a subsequent increase for M_{0-100}. The swelling ratio is a thermodynamic quantity measured at equilibrium between fully swollen and fully collapsed particles. This is

therefore a surprising result, indicating that the collapsed microgels maintain a memory of the transition, with a decreased deswelling for more heterogeneous networks even well-above their respective VPT. The smaller deswelling indicates that copolymer microgels detain more water at high temperatures. As a consequence, they are effectively stiffer with respect to their temperature response, being more able to resist the induced collapse. We also note that once again the difference between homopolymer PNIPAM and PNIPMAM microgels is in line with what observed in the literature.[26,41]

Conclusions

We have combined DLS, DSC, SANS and monomer-resolved numerical simulations to unravel how comonomer ratio governs the internal architecture and resulting thermoresponsive behavior of P(NIPAM-*co*-NIPMAM) copolymer microgels. While T_{VPT} increases with increasing NIPMAM content, its deviation from the expected value in case of a linear dependence on composition, as well as the non-monotonic broadening of the transition, hint that the polymer network conformation changes in a non-trivial way with composition and in response to the stimulus. Insights at the nanoscale were obtained from SANS analysis. The temperature evolution of the polymer mesh correlation length ζ, obtained from fitting of the form factors, indicates an increase in network heterogeneity at the onset of collapse, followed by a sharp decrease in the collapsed state. The increase of ζ below T_{VPT} is universal for all compositions investigated and identifies a regime of enhanced structural heterogeneity associated with the coexistence of collapsed and swollen domains.

Exploiting isotopic labelling and comparison with simulations, we provide evidence that radical copolymerization leads to the formation of a block-like internal topology composed of small domains containing mainly NIPAM or NIPMAM, rather than a random monomer distribution, as already pointed out in the case of P(NIPAM-*co*-NIPMAM) microgels of equimolar compositions.[28] As a consequence, ζ can be interpreted as the average spacing between

NIPAM-rich domains that collapse first owing to their lower VPTT. The non-monotonic dependence of ζ_{max} with composition, peaking at 75 mol % NIPMAM, demonstrates that copolymer microgels develop maximal internal segregation when NIPAM is present in a minor yet sufficient amount to form discrete responsive domains, which are separated by increasingly large non-collapsing PNIPMAM regions. Interestingly, the ζ_{max} trend is mirrored by the equilibrium swelling ratio, both experimentally and in silico, revealing that the fully collapsed state retains a structural memory of the heterogeneous transition pathway. Specifically, copolymer microgels with increased heterogeneity exhibit reduced deswelling, indicating an effectively less compliant network in response to temperature variations. Future works could focus on quantifying the microgel's bulk modulus as a function of NIPMAM content investigating whether the decreased swelling ratio for more heterogeneous networks translates into stiffer particles also in their swollen state.

Overall, these findings establish a direct link between mesoscale internal organization and macroscopic thermodynamic response, highlighting that copolymer microgel functionality is encoded not only in its chemical composition but also in the spatial monomer distribution, a detail often overlooked in copolymer systems. More broadly, this indicates how engineering the internal architecture allows tailoring their response by modulating their transition and deswelling, thereby enabling fine control over mechanical properties and stimuli responsiveness of interest in applications ranging from sensing to drug delivery and additive manufacturing.

Acknowledgement

The authors thank M. Bertoldo for valuable discussions. We acknowledge RAL for time at the SANS2D beamline under proposals 2310267 and 2320109 (data available at DOI: https://doi.org/10.5286/ISIS.E.RB2310267 and https://doi.org/10.5286/ISIS.E.RB2320109). We acknowledge Najet Mahmoudi for assistance during the experiments. This work is

based on experiments performed at the Swiss spallation neutron source SINQ, Paul Scherrer Institute, Villigen, Switzerland, instrument SANS-I, proposal 20220847. We acknowledge Urs Gasser for assistance during the experiments. This work benefited from the use of the SasView project (www.sasview.org), originally developed under NSF award DMR-0520547 and containing code developed with funding from the European Union's Horizon 2020 research and innovation programme under the SINE2020 project, grant agreement No 654000. The authors gratefully acknowledge the financial support of Consiglio Nazionale delle Ricerche within CNR-STFC Agreement 2021-2027 (N 0065606), concerning collaboration in scientific research 2310267 and 2320109 at the ISIS Neutron and Muon Source (UK) of Science and Technology Facilities Council (STFC). J.V. acknowledges funding from Ministero dell'Università e della Ricerca through the Rita Levi Montalcini research program (D.M. 1317 published on 15-12-2021, grant Nr. PGR21W3GY8). M.L. and E.Z. acknowledge financial support by Progetto Co-MGELS funded by the European Union - NextGeneration EU under the National Recovery and Resilience Plan Mission 4 "Istruzione e Ricerca" - Component C2 - Investment 1.1 - "Fondo PRIN", Project code PRIN2022PAYLXW Sector PE11, CUP B53D23008890006.

Conflict of Interest

The authors declare no conflict of interest.

Supporting Information Available

The Supporting Information is available free of charge at:

The Supporting Information contains: values of the parameters obtained by fitting the experimental swelling from DLS data; DSC thermograms; SANS scattering intensities, fits and resulting parameters as a function of temperature for all the investigated copolymer microgels; comparisons between experimental and numerical form factors; correlation length of

the polymer mesh (ζ) for M_{25-75} microgels containing H-NIPAM or D-NIPAM.

References

(1) Karg, M.; Pich, A.; Hellweg, T.; Hoare, T.; Lyon, L. A.; Crassous, J. J.; Suzuki, D.; Gumerov, R. A.; Schneider, S.; Potemkin, I. I.; Richtering, W. Nanogels and Microgels: From Model Colloids to Applications, Recent Developments, and Future Trends. *Langmuir* **2019**, *35*, 6231–6255.

(2) Highley, C. B.; Song, K. H.; Daly, A. C.; Burdick, J. A. Jammed Microgel Inks for 3D Printing Applications. *Advanced Science* **2019**, *6*, 1801076.

(3) Rey, M.; Fernandez-Rodriguez, M. A.; Karg, M.; Isa, L.; Vogel, N. Poly- N -isopropylacrylamide Nanogels and Microgels at Fluid Interfaces. *Accounts of Chemical Research* **2020**, *53*, 414–424.

(4) Xie, T.; Wang, H.; Li, J.; Xuan, L.; Nazir, F.; Chen, L.; Luo, Z.; Wang, M.; Miao, Y.; Zhang, D.; Li, W.; Tang, G. Microgels for 3D Biofabrication. *Aggregate* **2025**, *6*.

(5) Plamper, F. A.; Richtering, W. Functional Microgels and Microgel Systems. *Accounts of Chemical Research* **2017**, *50*, 131–140.

(6) Hertle, Y.; Hellweg, T. Thermoresponsive copolymer microgels. *Journal of Materials Chemistry B* **2013**, *1*, 5874.

(7) Kratz, K.; Hellweg, T.; Eimer, W. Influence of charge density on the swelling of colloidal poly(N-isopropylacrylamide-co-acrylic acid) microgels. *Colloids and Surfaces A: Physicochemical and Engineering Aspects* **2000**, *170*, 137–149.

(8) Del Monte, G.; Truzzolillo, D.; Camerin, F.; Ninarello, A.; Chauveau, E.; Tavagnacco, L.; Gnan, N.; Rovigatti, L.; Sennato, S.; Zaccarelli, E. Two-step deswelling

in the Volume Phase Transition of thermoresponsive microgels. *Proceedings of the National Academy of Sciences* **2021**, *118*, e2109560118.

(9) Phua, D. I.; Herman, K.; Balaceanu, A.; Zakrevski, J.; Pich, A. Reversible Size Modulation of Aqueous Microgels via Orthogonal or Combined Application of Thermo- and Phototriggers. *Langmuir* **2016**, *32*, 3867–3879.

(10) Hu, C.; Sun, Y.; van Wissen, G.; Peng, Y.; Pich, A. Visible Light-Responsive Microgels Modified with Donor–Acceptor Stenhouse Adducts. *Chemistry of Materials* **2022**, *34*, 4774–4784.

(11) Keerl, M.; Pedersen, J. S.; Richtering, W. Temperature Sensitive Copolymer Microgels with Nanophase Separated Structure. *Journal of the American Chemical Society* **2009**, *131*, 3093–3097.

(12) Clarke, K. C.; Lyon, L. A. Modulation of the Deswelling Temperature of Thermoresponsive Microgel Films. *Langmuir* **2013**, *29*, 12852–12857.

(13) Wiehemeier, L.; Cors, M.; Wrede, O.; Oberdisse, J.; Hellweg, T.; Kottke, T. Swelling behaviour of core-shell microgels in H2O, analysed by temperature-dependent FTIR spectroscopy. *Physical Chemistry Chemical Physics* **2019**, *21*, 572–580.

(14) Clara-Rahola, J.; Fernandez-Nieves, A.; Sierra-Martin, B.; South, A. B.; Lyon, L. A.; Kohlbrecher, J.; Barbero, A. F. Structural properties of thermoresponsive poly(N -isopropylacrylamide)-poly(ethyleneglycol) microgels. *The Journal of Chemical Physics* **2012**, *136*, 214903.

(15) Wellert, S.; Radulescu, A.; Carl, A.; Klitzing, R. V.; Gawlitza, K. Evolution of Size and Structure during the Polymerization Process: A SANS Study on EG-Based Microgels. *Macromolecules* **2015**, *48*, 4901–4909.

(16) Motlaq, V. F.; Knudsen, K. D.; Nyström, B. Effect of PEGylation on the stability of thermoresponsive nanogels. *Journal of Colloid and Interface Science* **2018**, *524*, 245–255.

(17) Agnihotri, P.; Raj, R.; Kumar, D.; Dan, A. Short oligo(ethylene glycol) chain incorporated thermoresponsive microgels: from structural analysis to modulation of solution properties. *Soft Matter* **2020**, *16*, 7845–7859.

(18) Vialetto, J.; Emerse, M.; Bassu, G.; Allgaier, J.; Laurati, M. Controlling the structure of star-like copolymer microgels through the monomer chain length to modulate softness and deswelling. *Journal of Colloid and Interface Science* **2026**, *703*, 139162.

(19) Kuroki, H.; Tokarev, I.; Minko, S. Responsive Surfaces for Life Science Applications. *Annual Review of Materials Research* **2012**, *42*, 343–372.

(20) Berndt, I.; Pedersen, J. S.; Richtering, W. Temperature-Sensitive Core–Shell Microgel Particles with Dense Shell. *Angewandte Chemie International Edition* **2006**, *45*, 1737–1741.

(21) Keerl, M.; Smirnovas, V.; Winter, R.; Richtering, W. Interplay between Hydrogen Bonding and Macromolecular Architecture Leading to Unusual Phase Behavior in Thermosensitive Microgels. *Angewandte Chemie International Edition* **2008**, *47*, 338–341.

(22) Hu, X.; Tong, Z.; Lyon, L. A. Multicompartment Core/Shell Microgels. *Journal of the American Chemical Society* **2010**, *132*, 11470–11472.

(23) Balaceanu, A.; Mayorga, V.; Lin, W.; Schürings, M. P.; Demco, D. E.; Böker, A.; Winnik, M. A.; Pich, A. Copolymer microgels by precipitation polymerisation of N-vinylcaprolactam and N-isopropylacrylamides in aqueous medium. *Colloid and Polymer Science* **2013**, *291*, 21–31.

(24) Duracher, D.; Elaïssari, A.; Pichot, C. Preparation of Poly(N-isopropylmethacrylamide) Latexes Kinetic Studies and Characterization. *J Polym Sci A: Polym Chem* **1999**, *37*, 1823–1837.

(25) Hoare, T.; McLean, D. Kinetic prediction of functional group distributions in thermosensitive microgels. *Journal of Physical Chemistry B* **2006**, *110*, 20327–20336.

(26) Wedel, B.; Hertle, Y.; Wrede, O.; Bookhold, J.; Hellweg, T. Smart Homopolymer Microgels: Influence of the Monomer Structure on the Particle Properties. *Polymers* **2016**, *8*, 162.

(27) Djokpé, E.; Vogt, W. N-Isopropylacrylamide andN-Isopropylmethacryl-amide: Cloud Points of Mixtures and Copolymers. *Macromolecular Chemistry and Physics* **2001**, *202*, 750–757.

(28) Tavagnacco, L.; Buratti, E.; Vialetto, J.; Brasili, F.; Ballin, E.; Schwärzer, K.; Mata, J.; Carmine, G. D.; Bertoldo, M.; Chiessi, E.; Laurati, M.; Zaccarelli, E. Thermoresponsive Copolymer Microgels Synthesized via Single-Step Precipitation Polymerization: Random or Block Structure? *Small* **2025**, *21*.

(29) Monte, G. D.; Truzzolillo, D.; Camerin, F.; Ninarello, A.; Chauveau, E.; Tavagnacco, L.; Gnan, N.; Rovigatti, L.; Sennato, S.; Zaccarelli, E. Two-step deswelling in the Volume Phase Transition of thermoresponsive microgels. *Proceedings of the National Academy of Sciences* **2021**, *118*, e2109560118.

(30) Ballin, E.; Brasili, F.; Papetti, T.; Vialetto, J.; Sztucki, M.; Sennato, S.; Laurati, M.; Zaccarelli, E. Star-like thermoresponsive microgels as an emerging class of soft nanocolloids. *ACS nano* **2025**, *19*, 35447–35458.

(31) Stieger, M.; Richtering, W.; Pedersen, J. S.; Lindner, P. Small-angle neutron scattering study of structural changes in temperature sensitive microgel colloids. *The Journal of Chemical Physics* **2004**, *120*, 6197–6206.

(32) Bassu, G.; Houston, J. E.; Lara-Peña, M. A.; Kriegs, H.; Lettinga, M. P.; Porcar, L.; Scotti, A.; Laurati, M. Link between permanent shear-banding and local concentration fluctuations in suspensions of compressible microgels. *Physics of Fluids* **2024**, *36*, 113116.

(33) Pedersen, J. S. Resolution effects and analysis of small-angle neutron scattering data. *J. Phys. IV France* **1993**, *03*, C8–491–C8–498.

(34) Gnan, N.; Rovigatti, L.; Bergman, M.; Zaccarelli, E. In silico synthesis of microgel particles. *Macromolecules* **2017**, *50*, 8777–8786.

(35) Ninarello, A.; Crassous, J. J.; Paloli, D.; Camerin, F.; Gnan, N.; Rovigatti, L.; Schurtenberger, P.; Zaccarelli, E. Modeling microgels with a controlled structure across the volume phase transition. *Macromolecules* **2019**, *52*, 7584–7592.

(36) Grest, G. S.; Kremer, K. Molecular dynamics simulation for polymers in the presence of a heat bath. *Physical Review A* **1986**, *33*, 3628.

(37) Soddemann, T.; Dünweg, B.; Kremer, K. A generic computer model for amphiphilic systems. *The European Physical Journal E* **2001**, *6*, 409–419.

(38) Plimpton, S. Fast parallel algorithms for short-range molecular dynamics. *Journal of computational physics* **1995**, *117*, 1–19.

(39) Hubbard, J. B.; Douglas, J. F. Hydrodynamic friction of arbitrarily shaped Brownian particles. *Physical Review E* **1993**, *47*, R2983.

(40) Djokpé, E.; Vogt, W. N-Isopropylacrylamide and N-Isopropylmethacryl-amide: Cloud Points of Mixtures and Copolymers. *Macromolecular Chemistry and Physics* **2001**, *202*, 750–757.

(41) Cors, M.; Wiehemeier, L.; Oberdisse, J.; Hellweg, T. Deuteration-induced volume phase transition temperature shift of PNIPMAM microgels. *Polymers* **2019**, *11*, 620.

(42) Matsui, S.; Nishizawa, Y.; Uchihashi, T.; Suzuki, D. Monitoring Thermoresponsive Morphological Changes in Individual Hydrogel Microspheres. *ACS Omega* **2018**, *3*, 10836–10842.

(43) Nishizawa, Y.; Matsui, S.; Urayama, K.; Kureha, T.; Shibayama, M.; Uchihashi, T.; Suzuki, D. Non-Thermoresponsive Decanano-sized Domains in Thermoresponsive Hydrogel Microspheres Revealed by Temperature-Controlled High-Speed Atomic Force Microscopy. *Angewandte Chemie* **2019**, *131*, 8901–8905.

Supporting information for:

Heterogeneous collapse in thermoresponsive copolymer microgels varying molar composition

Table S2: Fitting parameters of the experimental swelling curve to eq. 1.

sample	T_{VPT} (°C)	$1/s$ (°C)	R_{max} (nm)	ΔR (nm)	A (nm/°C)	B (10^{-3} nm/°C^2)
M_{100-0}	33.1 ± 0.1	2.36 ± 0.13	41.4 ± 0.1	9.3 ± 0.3	-0.45 ± 0.02	13.9 ± 1.0
M_{75-25}	35.0 ± 0.1	2.73 ± 0.12	53.2 ± 0.2	13.6 ± 0.4	-0.32 ± 0.03	10.1 ± 1.3
$M_{62.5-37.5}$	36.1 ± 0.1	2.67 ± 0.13	59.2 ± 0.2	14.4 ± 0.4	-0.36 ± 0.04	11.4 ± 1.5
M_{50-50}	37.9 ± 0.1	2.60 ± 0.11	63.3 ± 0.1	14.5 ± 0.3	-0.36 ± 0.02	8.6 ± 0.6
$M_{37.5-62.5}$	39.2 ± 0.1	2.68 ± 0.11	52.7 ± 0.1	11.1 ± 0.2	-0.31 ± 0.01	7.5 ± 0.4
M_{25-75}	40.9 ± 0.1	2.98 ± 0.12	75.9 ± 0.2	16.7 ± 0.3	-0.30 ± 0.03	7.2 ± 0.8
M_{0-100}	44.4 ± 0.1	3.90 ± 0.18	69.6 ± 0.2	18.2 ± 0.5	-0.22 ± 0.03	8.1 ± 0.8

Table S2 reports the values of the parameters obtained by fitting the experimental swelling curves of microgels at varying co-polymer compositions. The data and the fitting curves are plotted in Fig. 1B of the main text. The parameters T_{VPT} and $1/s$ are plotted as a function of the molar fraction of NIPMAM in Figs. 1C and 1D, respectively. The coefficients A and B, weight the linear and quadratic phenomenological terms in eq. 1, allowing the fitting function to accurately reproduce the experimental data while preserving the physical meaning of the relevant fitting parameters.

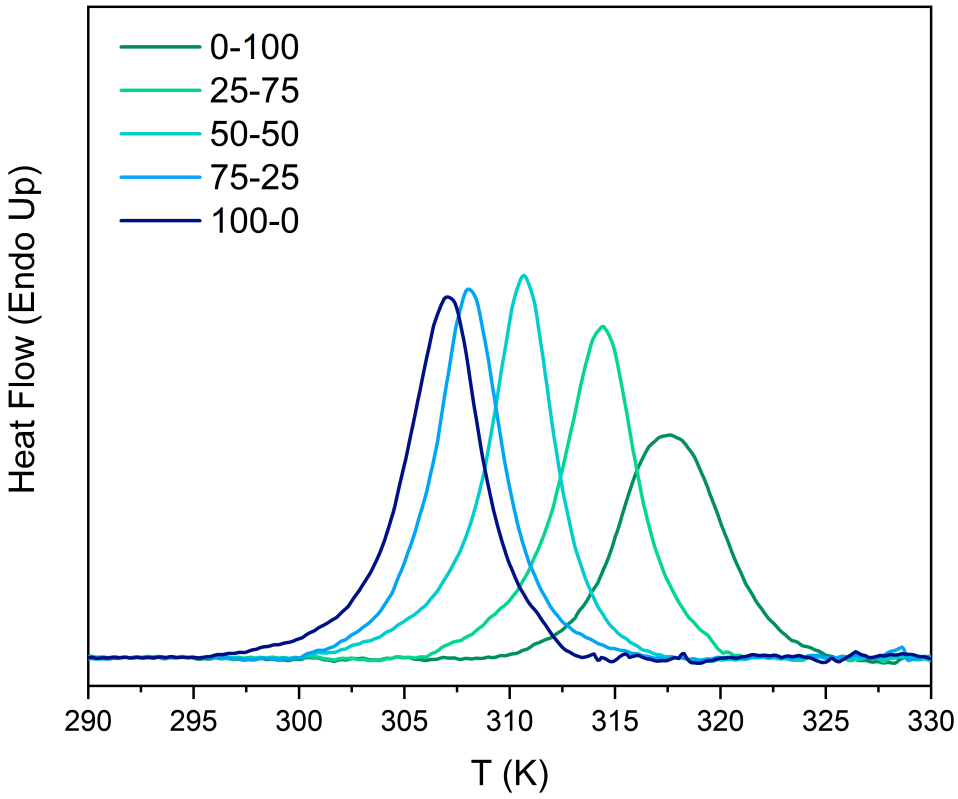


Figure S1: **Differential scanning calorimetry.** DSC thermograms for P(NIPAM-*co*-NIPMAM) microgels at varying mol fraction of the components, as indicated.

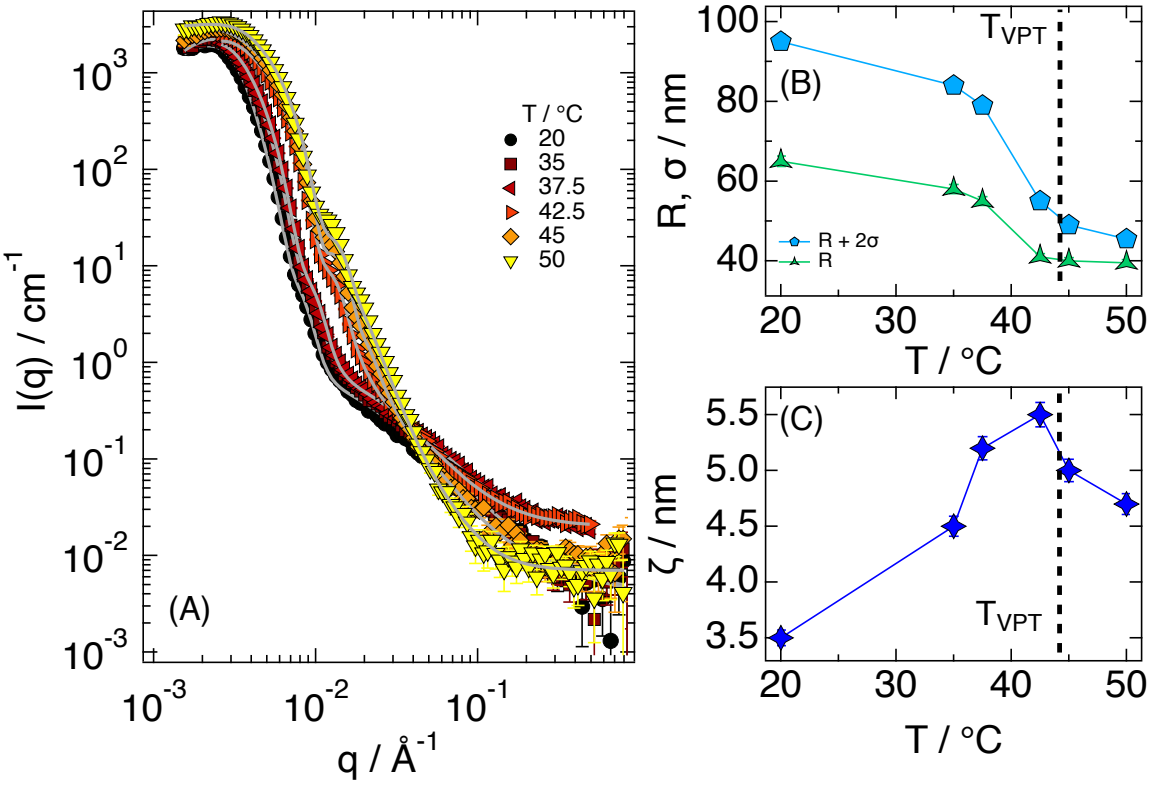


Figure S2: **SANS of $\mathbf{M}_{0-100}$.** Left: SANS scattering intensities $I(q)$ as a function of temperature. Lines represent fits with the fuzzy sphere model, including $S(q)$ contribution. Top-right: particle core radius (R) and total radius ($R + 2\sigma$) from SANS fits as a function of temperature. Bottom-right: correlation length of the polymer mesh (ζ). T_{VPT} (dashed line) indicates the VPTT from DLS analysis.

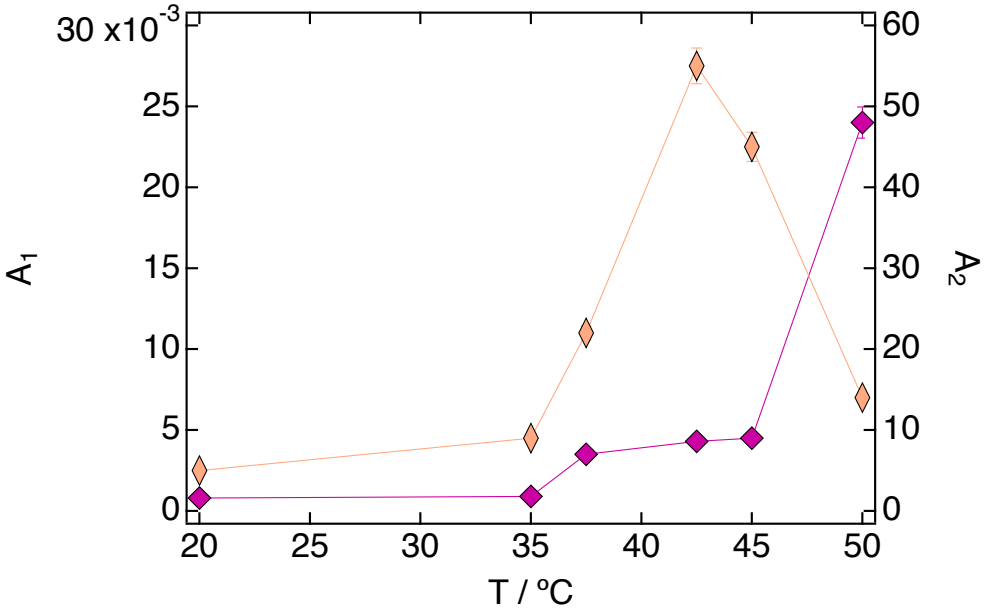


Figure S3: **SANS of $\mathbf{M}_{0-100}$.** Parameters A_1 (pink squares) and A_2 (orange diamonds) from SANS fits as a function of temperature.

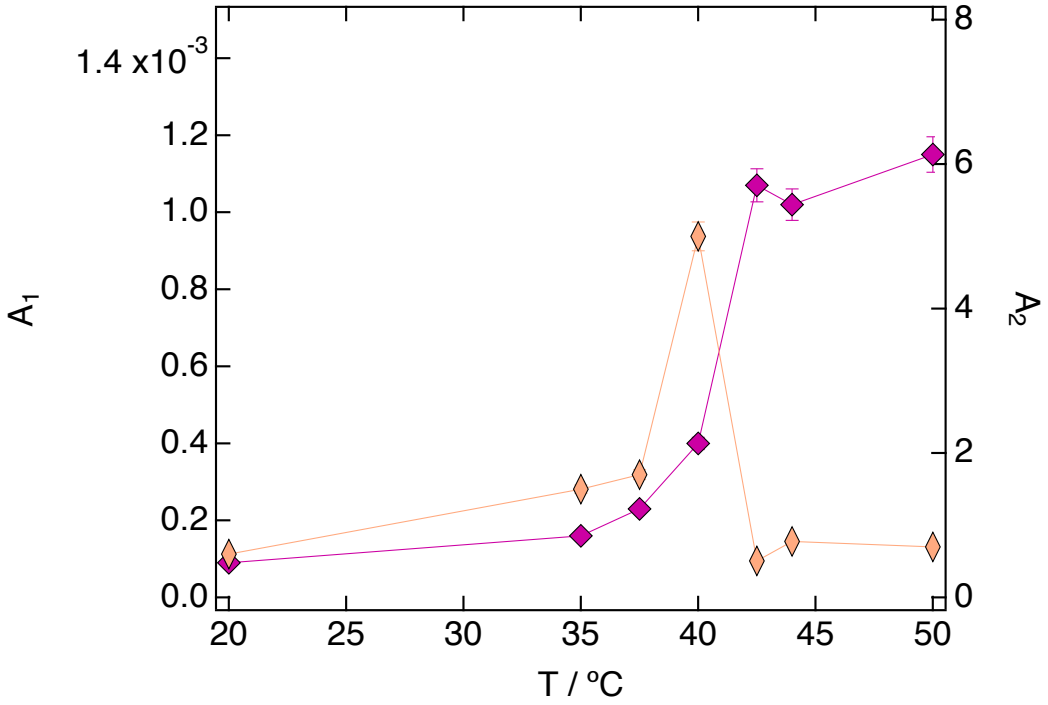


Figure S4: **SANS of $\mathbf{M}_{25-75}$.** Parameters A_1 (pink squares) and A_2 (orange diamonds) from SANS fits as a function of temperature.

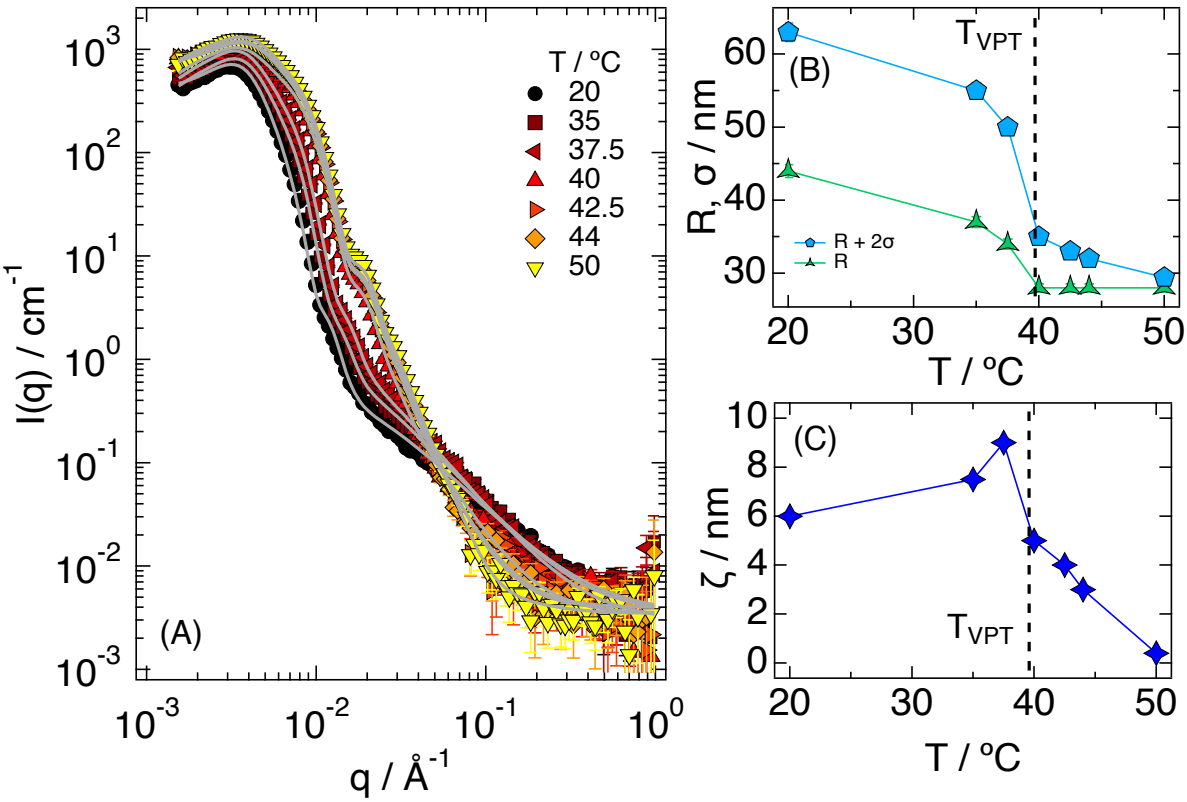


Figure S5: **SANS of $\mathbf{M}_{37.5-62.5}$.** Left: SANS scattering intensities $I(q)$ as a function of temperature. Lines represent fits with the fuzzy sphere model, including $S(q)$ contribution. Top-right: particle core radius (R) and total radius ($R + 2\sigma$) from SANS fits as a function of temperature. Bottom-right: correlation length of the polymer mesh (ζ). T_{VPT} (dashed line) indicates the VPTT from DLS analysis.

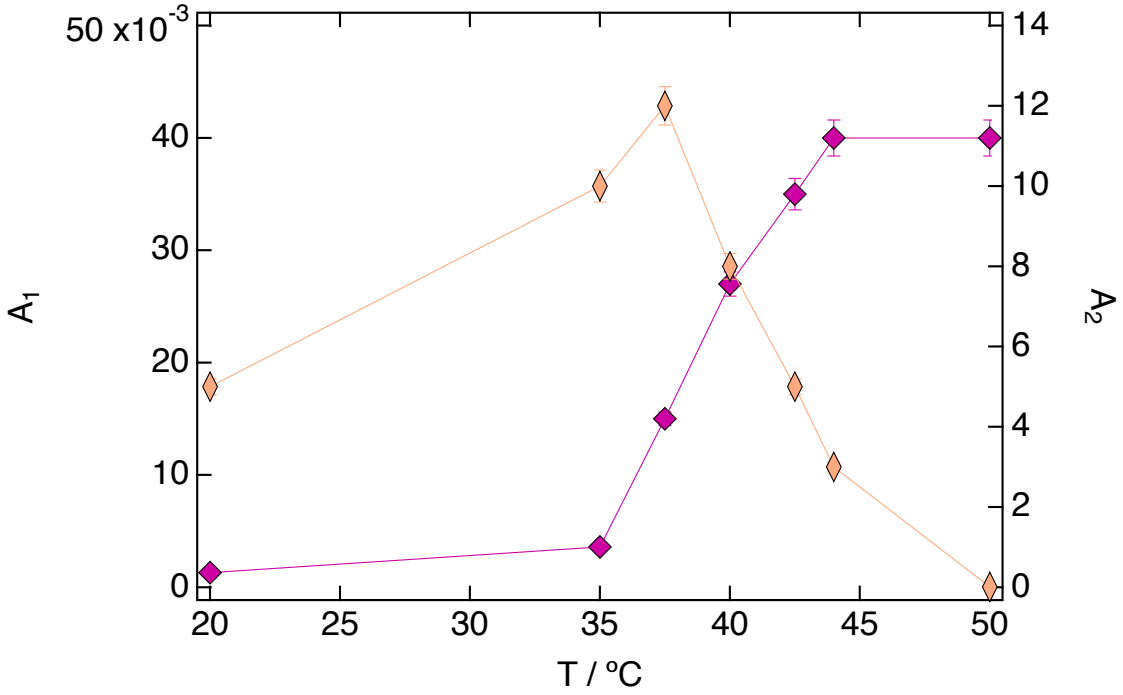


Figure S6: **SANS of $\mathbf{M}_{37.5-62.5}$.** Parameters A_1 (pink squares) and A_2 (orange diamonds) from SANS fits as a function of temperature.

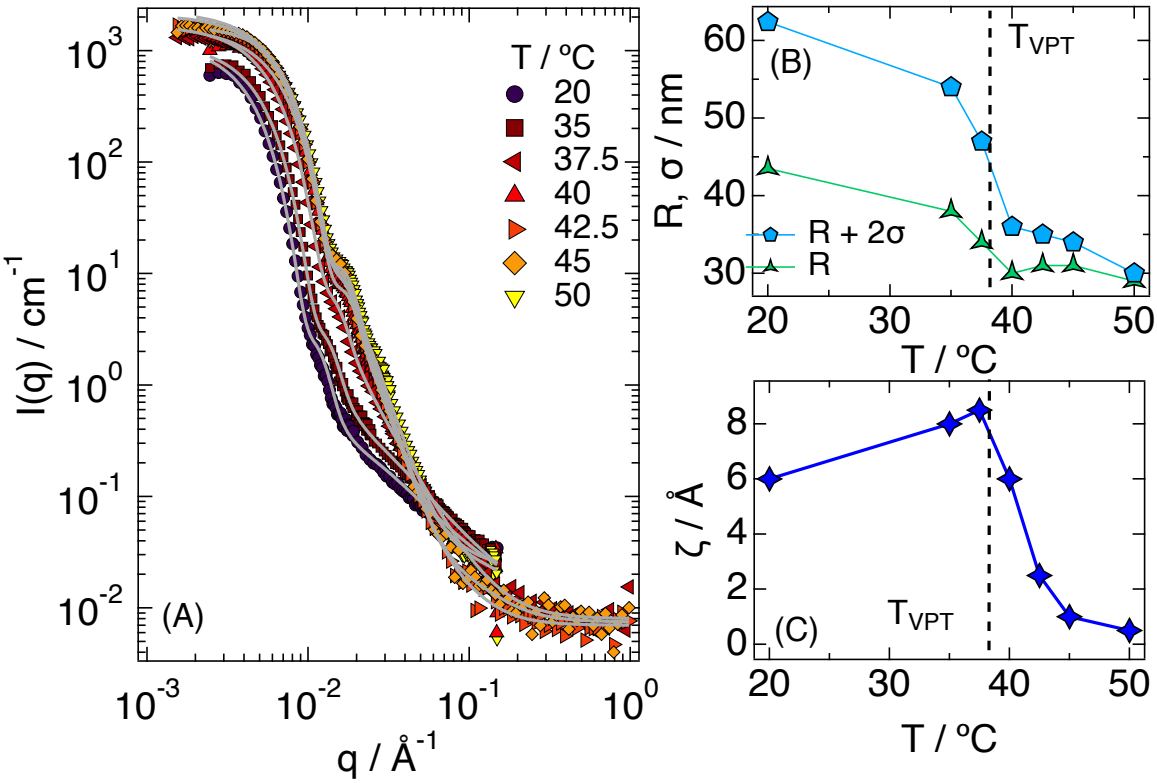


Figure S7: **SANS of $\mathbf{M}_{50-50}$.** Left: SANS scattering intensities $I(q)$ as a function of temperature. Lines represent fits with the fuzzy sphere model. Top-right: particle core radius (R) and total radius ($R + 2\sigma$) from SANS fits as a function of temperature. Bottom-right: correlation length of the polymer mesh (ζ). T_{VPT} (dashed line) indicates the VPTT from DLS analysis.

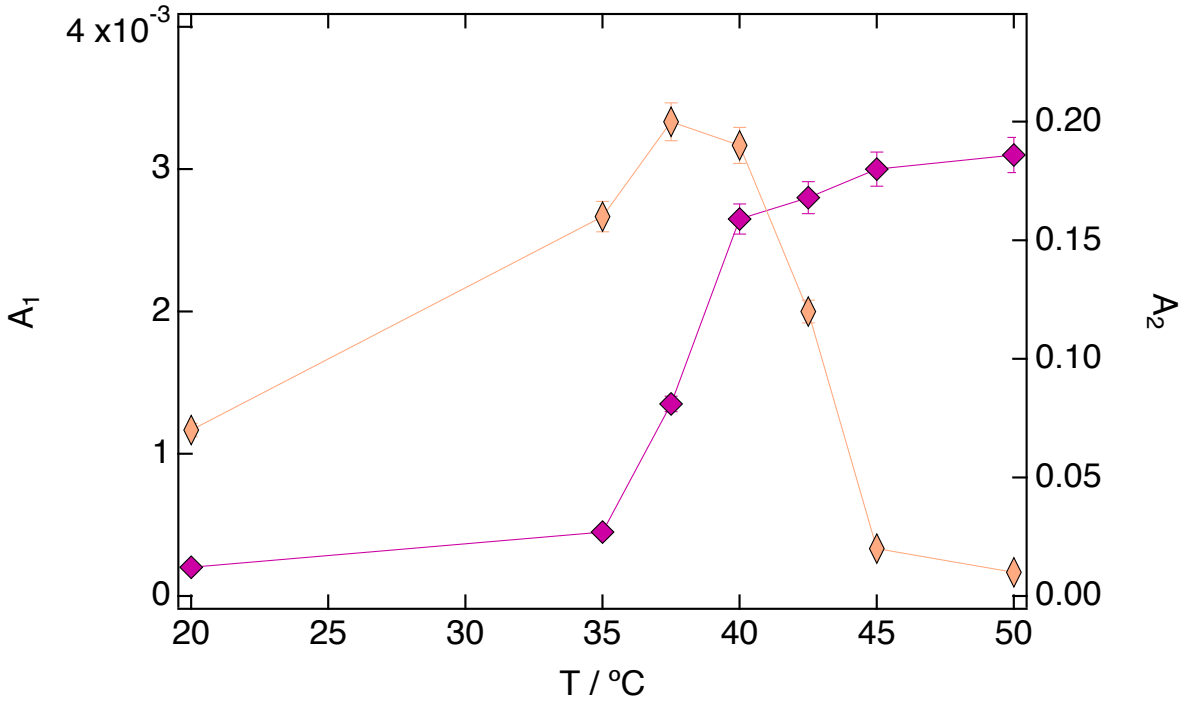


Figure S8: **SANS of $\mathbf{M}_{50-50}$.** Parameters A_1 (pink squares) and A_2 (orange diamonds) from SANS fits as a function of temperature.

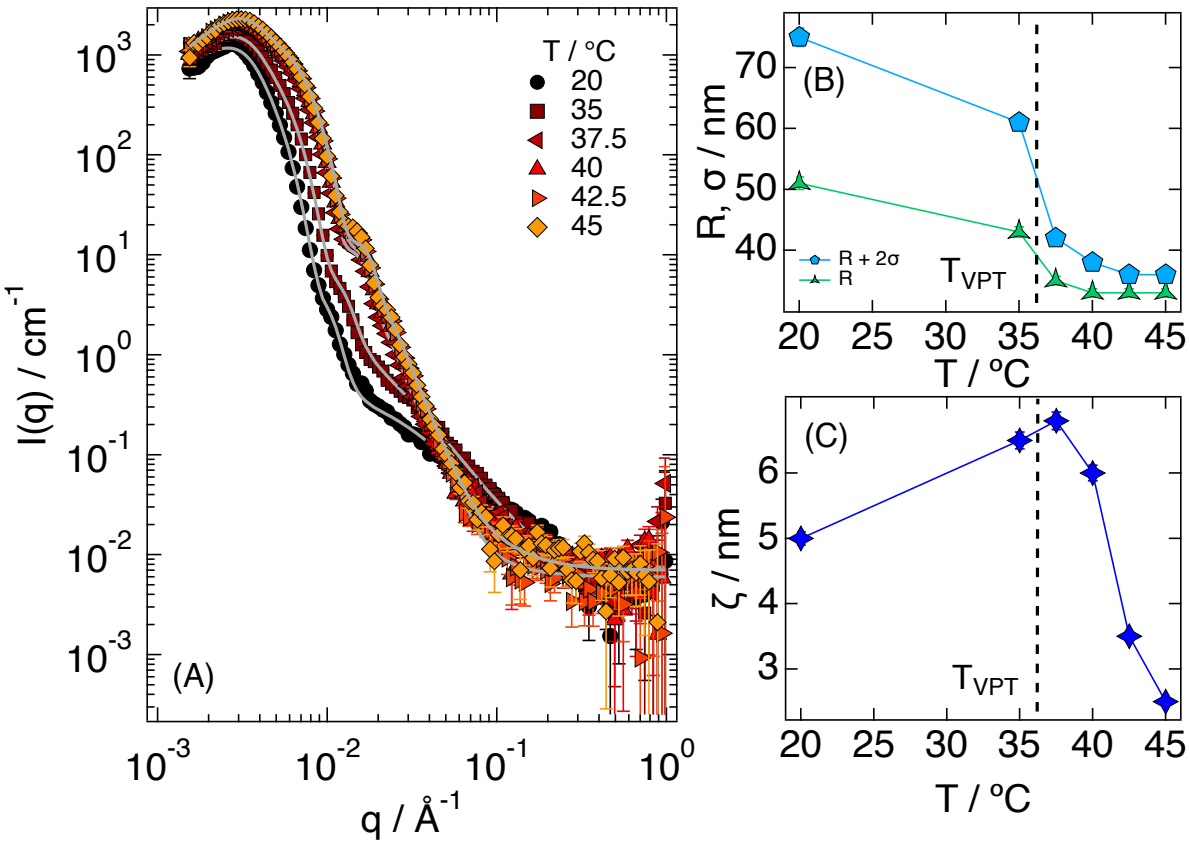


Figure S9: **SANS of $\mathbf{M}_{62.5-37.5}$.** Left: SANS scattering intensities $I(q)$ as a function of temperature. Lines represent fits with the fuzzy sphere model, including $S(q)$ contribution. Top-right: particle core radius (R) and total radius ($R + 2\sigma$) from SANS fits as a function of temperature. Bottom-right: correlation length of the polymer mesh (ζ). T_{VPT} (dashed line) indicates the VPTT from DLS analysis.

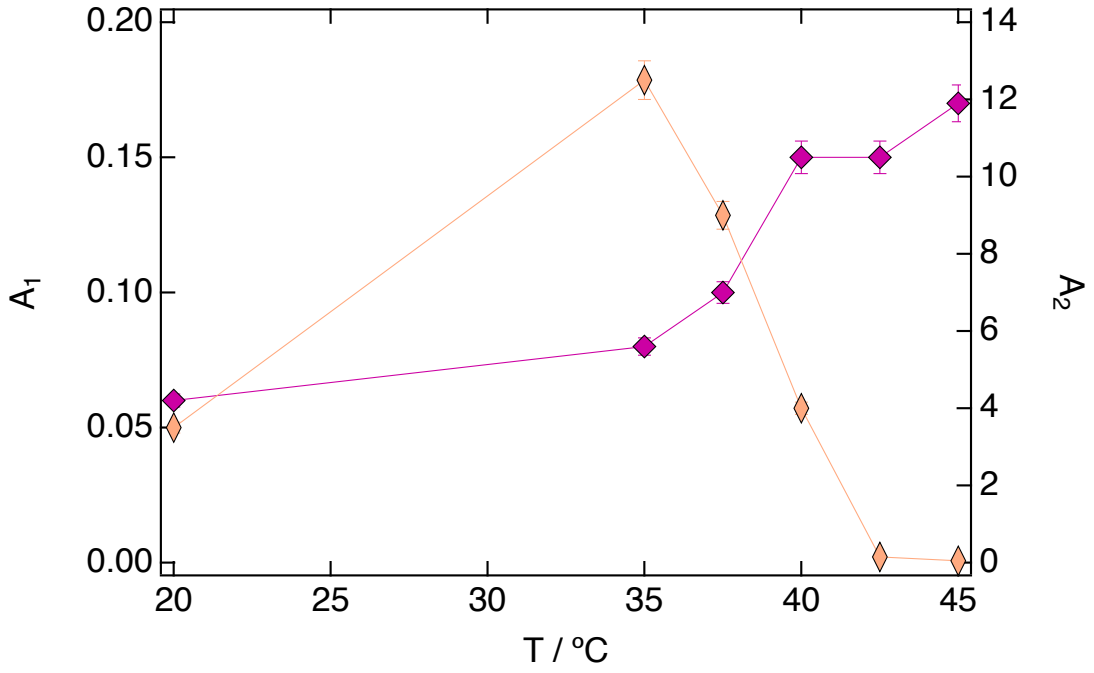


Figure S10: **SANS of $\mathbf{M}_{62.5-37.5}$.** Parameters A_1 (pink squares) and A_2 (orange diamonds) from SANS fits as a function of temperature.

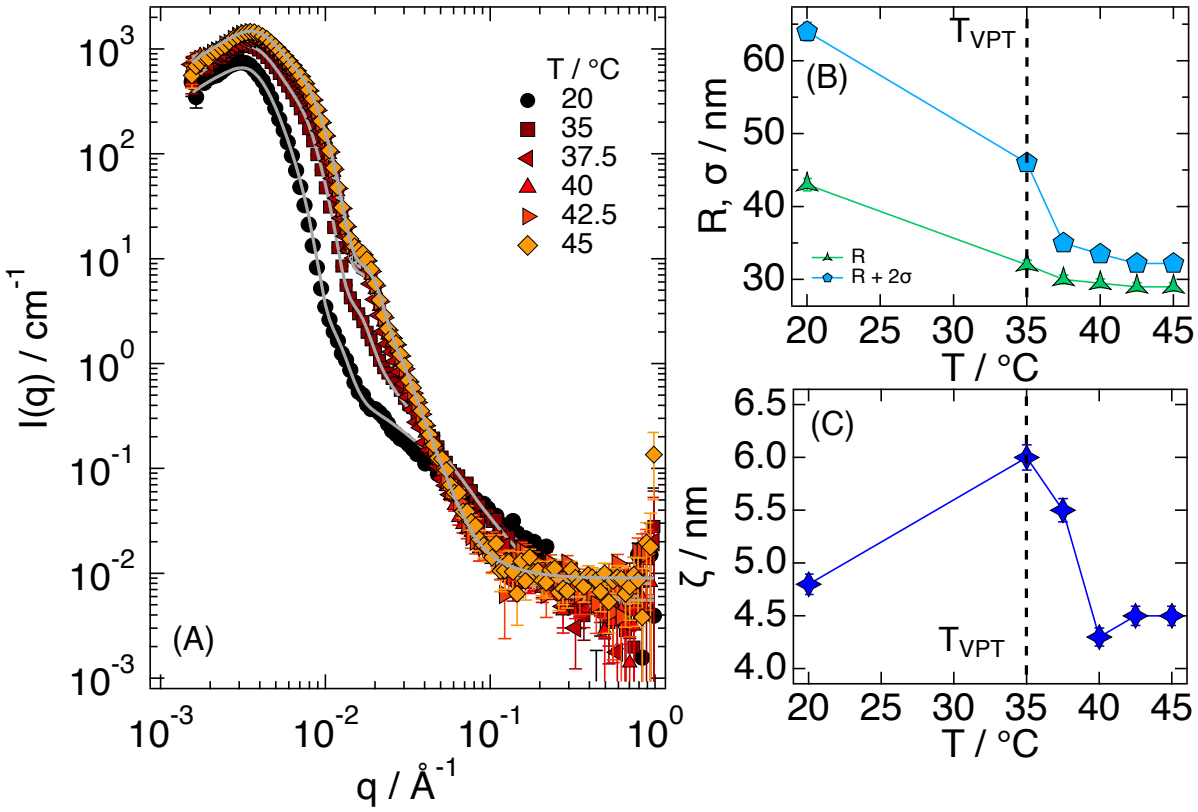


Figure S11: **SANS of $\mathbf{M}_{75-25}$.** Left: SANS scattering intensities $I(q)$ as a function of temperature. Lines represent fits with the fuzzy sphere model, including $S(q)$ contribution. Top-right: particle core radius (R) and total radius ($R + 2\sigma$) from SANS fits as a function of temperature. Bottom-right: correlation length of the polymer mesh (ζ). T_{VPT} (dashed line) indicates the VPTT from DLS analysis.

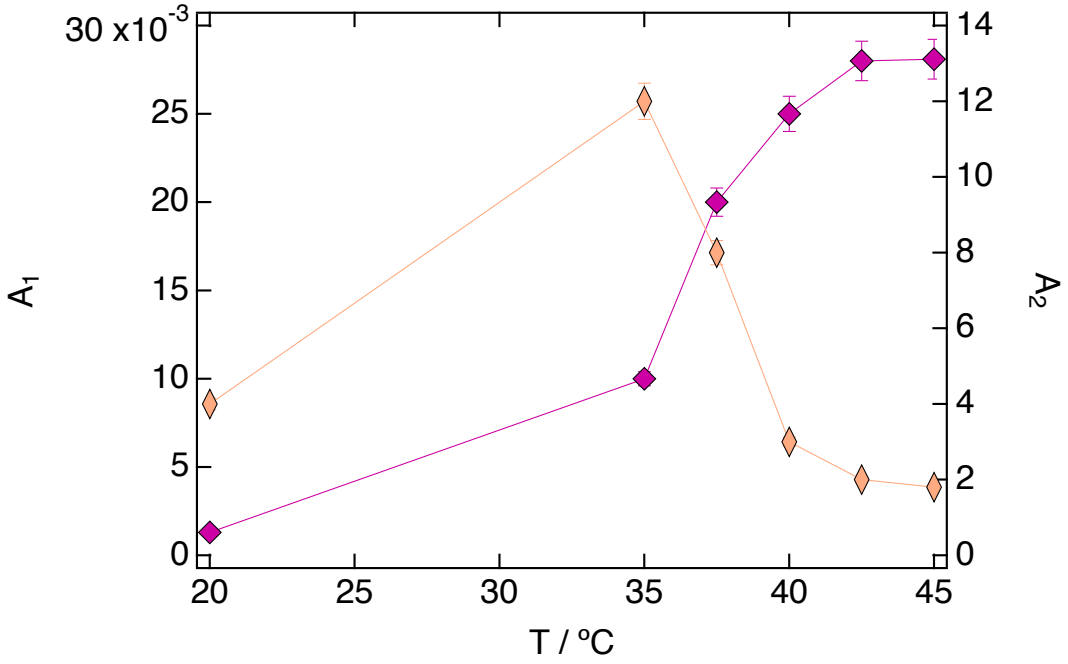


Figure S12: **SANS of $\mathbf{M}_{75-25}$.** Parameters A_1 (pink squares) and A_2 (orange diamonds) from SANS fits as a function of temperature.

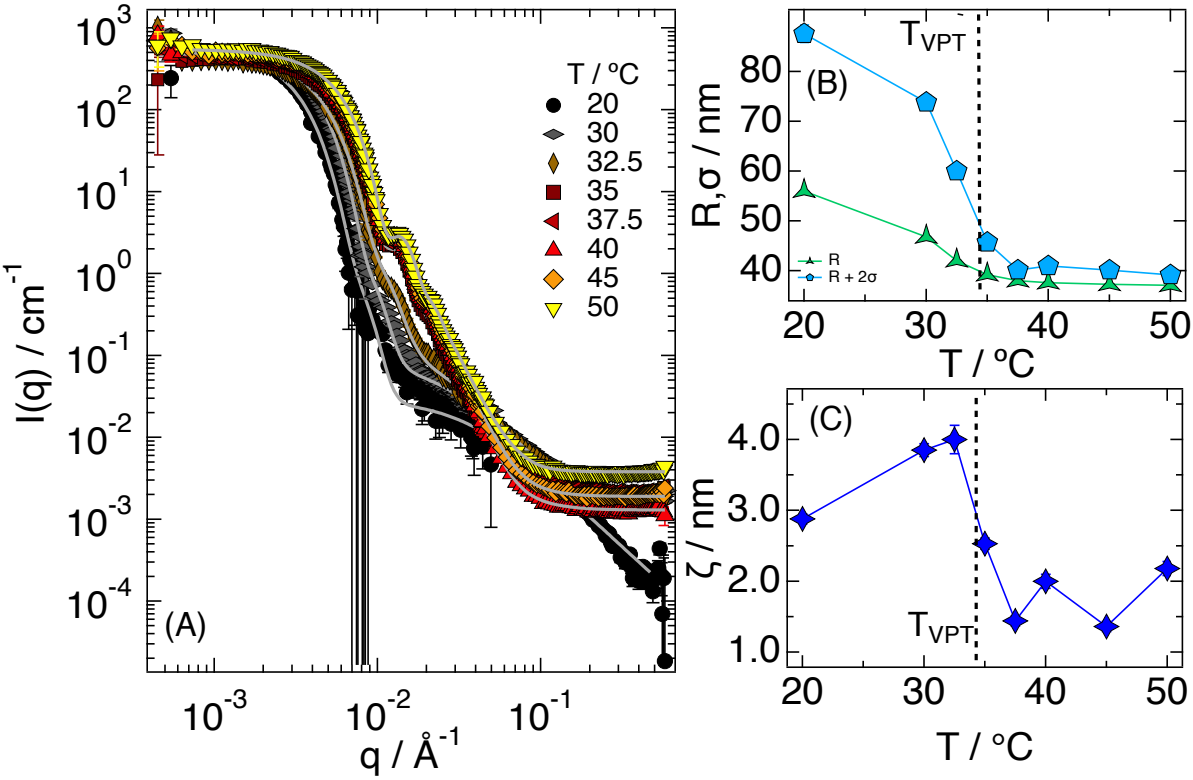


Figure S13: **SANS of $\mathbf{M}_{100-0}$.** Left: SANS scattering intensities $I(q)$ as a function of temperature. Lines represent fits with the fuzzy sphere model. Top-right: particle core radius (R) and total radius ($R + 2\sigma$) from SANS fits as a function of temperature. Bottom-right: correlation length of the polymer mesh (ζ). T_{VPT} (dashed line) indicates the VPTT from DLS analysis.

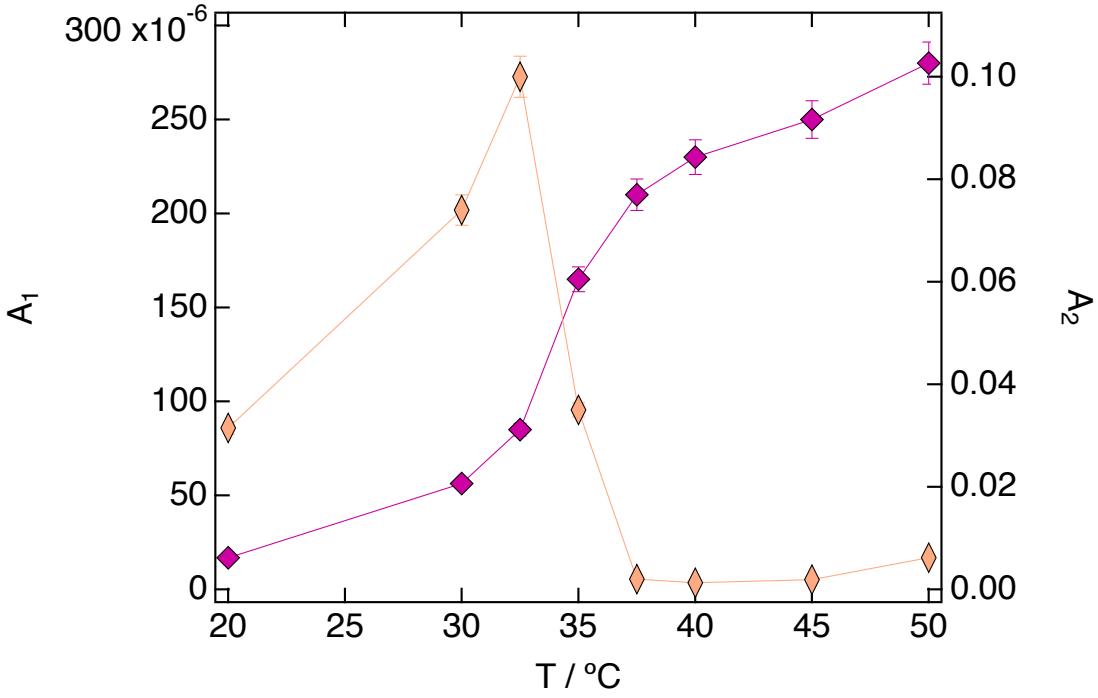


Figure S14: **SANS of $\mathbf{M}_{100-0}$.** Parameters A_1 (pink squares) and A_2 (orange diamonds) from SANS fits as a function of temperature.

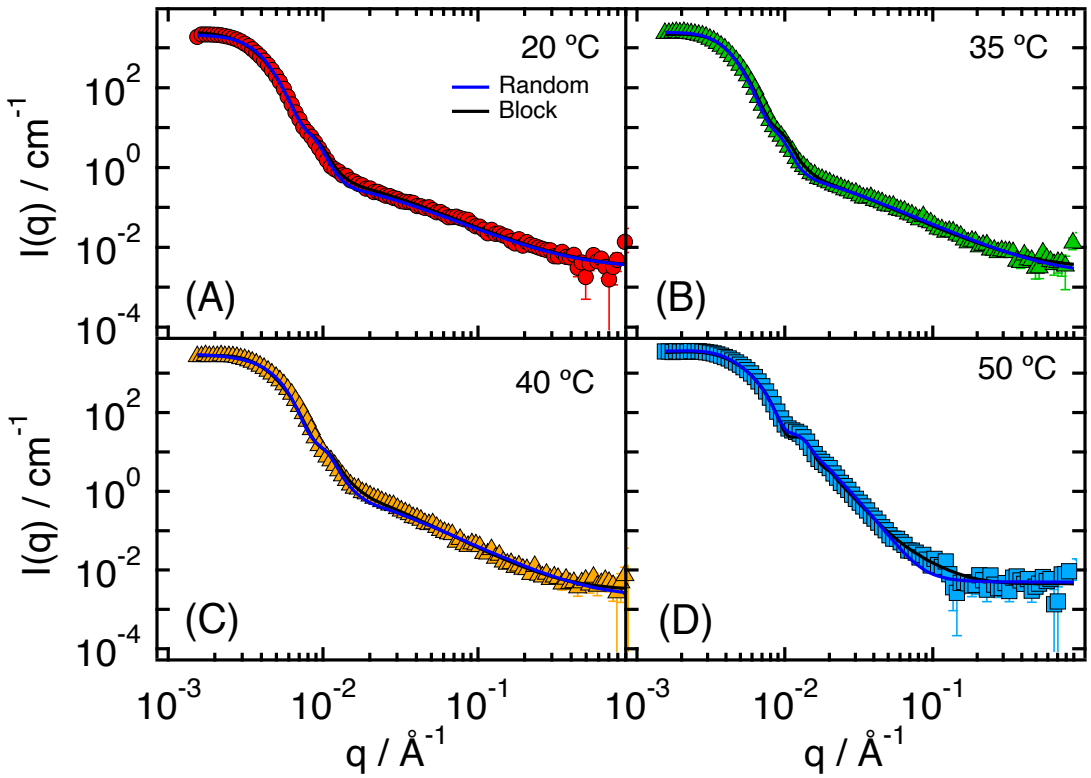


Figure S15: **Comparison between experimental and numerical form factors.** Experimental data (points) are measured for M_{25-75} microgels (P(H-NIPAM-*co*-H-NIPMAM)) at different temperatures. Black lines are numerical form factors obtained with the "*block*" model while blue lines are numerical form factors obtained with the "*random*" model (see Materials and Methods for details on the comparison procedure).

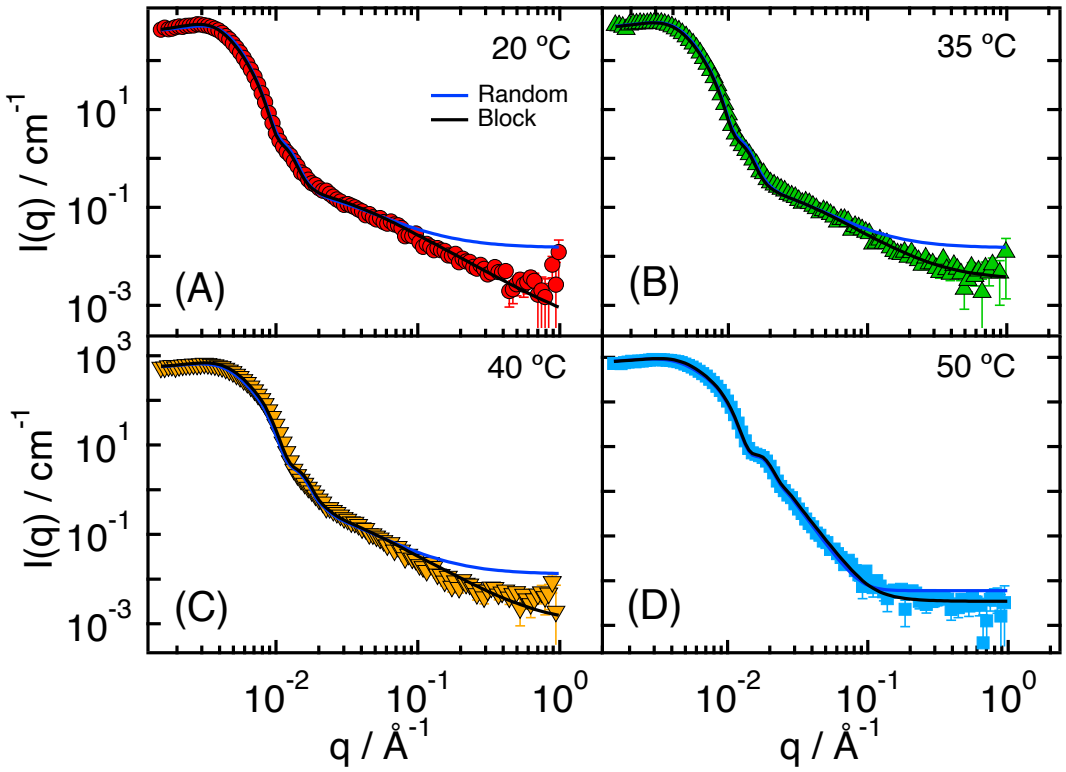


Figure S16: **Comparison between experimental and numerical form factors.** Experimental data (points) are measured for partially deuterated M_{25-75} microgels (P(D-NIPAM-*co*-H-NIPMAM)) at different temperatures. Black lines are numerical form factors obtained with the "*block*" model while blue lines are numerical form factors obtained with the "*random*" model (see Materials and Methods for details on the comparison procedure).

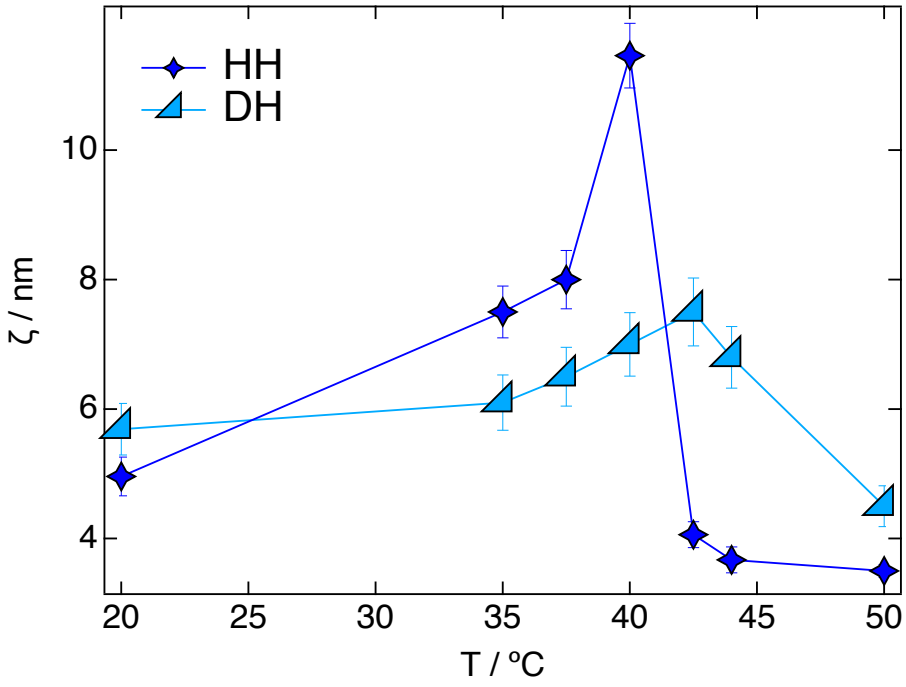
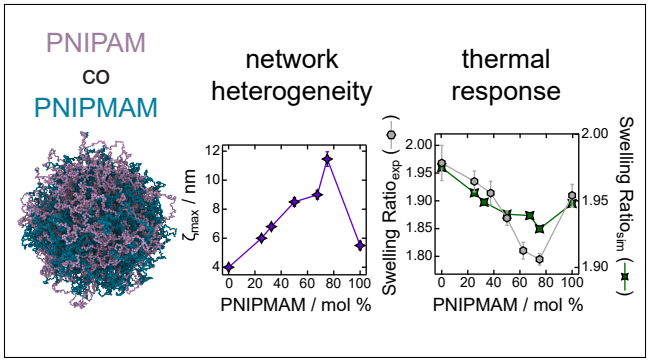


Figure S17: **Correlation length of the polymer mesh (ζ) for M_{25-75} microgels containing H-NIPAM (HH) or D-NIPAM (DH).**

TOC Graphic


PNIPAM
co
PNIPMAM
network
heterogeneity
thermal
response
ζ_{max} / nm
PNIPMAM / mol %
Swelling Ratio$_{exp}$ (—o—)
Swelling Ratio$_{sim}$ (—x—)
PNIPMAM / mol %